A Modular Robotic AFO for detecting phase changes during Walking Gait

by

Nathaniel Michaels

A Thesis

Submitted to the Faculty

of the

WORCESTER POLYTECHNIC INSTITUTE

In partial fulfillment of the requirements for the

Degree of Master of Science

in

Robotics Engineering

by

May 2020

APPROVED:

_____

Professor Gregory Fischer, Major Thesis Advisor

_____

Professor William Michalson, Thesis Committee

_____

Professor Mahdi Agheli, Thesis Committee

Abstract

The focus of this paper is on the development of a modular AFO (Ankle Foot Orthosis) subsystem for the greater L.A.R.R.E (Legged Anthropomorphic Robotic Rehab Exoskeleton) Exoskeleton. The main role of the AFO device is in the role of medical rehabilitation, by providing passively-powered dorsiflexion support to the user's ankle in order to prevent foot drop. It is able to accomplish this role through the use of a torsional spring attached to the ankle joint. Additionally, the AFO must also be able to provide sensory-feedback to the greater L.A.R.R.E system in order to help control walking gait. It can detect the orientation of the ankle through the use of both a potentiometer and IMU attached at the ankle joint, and it can detect which part of the foot is in contact with the ground through a specially-designed tactile sensor embedded within the sole of the AFO. This sensor consists of Force-Sensing Resistor sensors encased within a polyurethane rubber mold to provide protection from wear and tear as well as provide a rough surface to keep the device from slipping. The development of this "Sole-Sensor" was fairly extensive, with multiple iterations of the sensor being developed over the course of the project. It was found that Sole-Sensor works best when the resin geometry is shaped in such a way that it concentrates all forces applied on it directly above the FSRs. The development of a working Sole-Sensor subsystem allowed a proper test of the Right-foot AFO system within a VICON Motion-Capture room to test Foot-position detection and Center-of-Pressure point tracking. Translating the AFO CoP point into the VICON Lab's "World Frame" and comparing it to the independently calculated Force-Plate CoP point shows a maximum position displacement of $+/-3$cm along the AFO's X-axis and $+/-5$cm along the Y-axis.

Acknowledgements

I would like to thank my research advisor, Prof. Gregory Fischer, for helping me develop a clear research plan for this project, as well as providing much needed guidance and insight that helped resolve many of the issues during the development the Force-Sensitive Sole-Sensor sub-system.

I would also like to thank my exoskeleton project team members, Nathaniel Goldfarb and Vishnu Aishwaryan, without whom this device and the L.A.R.R.E system as a whole would not exist.

Contents

List of Figures

List of Tables

Chapter 1

Introduction and Project Background

1.1 L.A.R.R.E Exoskeleton System

The project discussed in this paper was developed as one part of the larger L.A.R.R.E (Legged Anthropomorphic Robotic Rehab Exoskeleton) system. The L.A.R.R.E. is a modular, lower-limb robotic exoskeleton, developed by Worcester Polytechnic Institute' Automative and Innovative Medicine Laboratory (WPI AIM Lab). The system is designed to help rehabilitate patients suffering from lower-limb or spinal cord injuries. Each joint of the exoskeleton, the Hip, Knee, and Ankle, are designed to be modular individual subsystems, such that they can all work independently from one another. This allows for relatively simple maintenance of the exoskeleton, making it possible to remove a single joint sub-system without having to disassemble the rest of the exoskeleton in the process. In the original design for the L.A.R.R.E, the only active component would be the Hip joint, while the Knee and Ankle joints provided passive support.

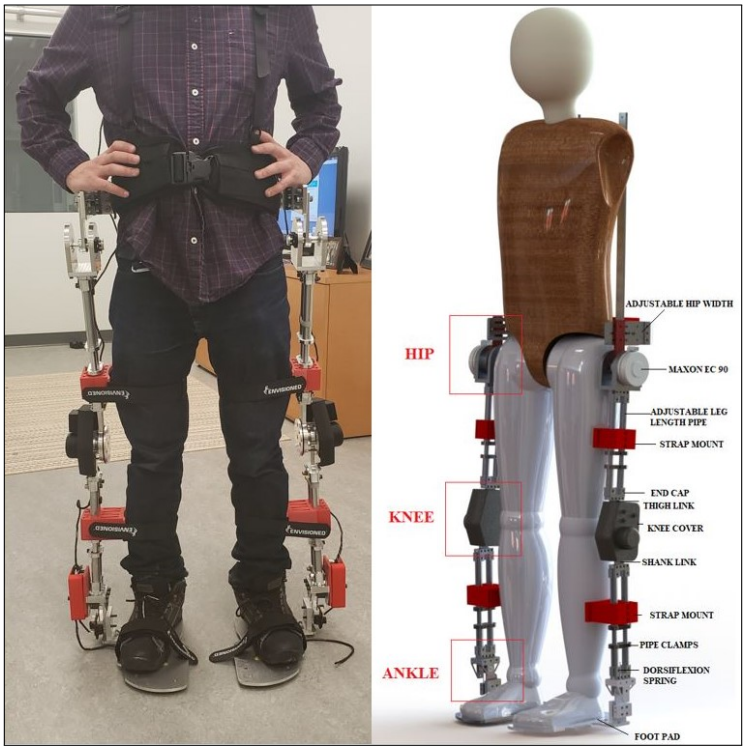

Figure 1.1: (Left) The completed L.A.R.R.E Exoskeleton System in use during routine testing. (Right) Labeled CAD model of the exoskeleton.

This project in particular focuses on the development of the modular Ankle-Joint System of the Exoskeleton. In order to maintain balance within the exoskeleton, the Ankle-Joint must provide some form of sensory input that tells L.A.R.R.E what position the foot is in at any point in time, whether or not it is currently in contact with the ground, and where the Center-of-Pressure point on each foot is located. This in turn will help the greater L.A.R.R.E system properly calculate the position of its Center-of-Mass, which is critical to know for Humanoid Robotic systems to keep themselves upright. The device is able to satisfy this requirement through a specially designed sensor installed at the sole, dubbed the Force-Sensing Sole-Sensor or just "Sole-Sensor". This particular sensor went through extensive development throughout this project, which is discussed in depth in Chapter 3 of this paper. In addition to the Sole-Sensor, the Ankle-Joint also has a potentiometer installed

within the Axle/Shaft component of the Ankle-Joint, in order for L.A.R.R.E to know the current orientation of the operator's ankle even when the foot is lifted off the ground. Finally, the Ankle-Joint must be also be able to fulfill these requirements all while supporting the combined weight of both the L.A.R.R.E and the operator.

Due to the modular nature of each joint, the ankle-portion should still be able to provide some form of rehabilitative support to the user on its own. This would qualify the Ankle sub-system as an Ankle-Foot Orthosis (AFO) device. As an AFO, the Ankle sub-system needs to be able to provide dorsiflexion motion support to the operator's ankle and help mitigate foot drop. "Dorsiflexion" is the act of raising the foot upwards towards the shin [1], which occurs frequently during the "toe-off" phase of the normal walking-gait cycle. Since it was decided that the Ankle joint should only provide passive support, a torsional spring is installed within the ankle joint. Later sections go into greater detail about the design, but in summary the torsional spring pulls the user's foot back into the default "flat-foot" position as soon as it starts to drop. In addition to preventing foot-drop, the AFO has an additional purpose within the greater L.A.R.R.E. system.

1.2 Background Research

1.2.1 Ankle-Foot Orthoses (AFO) Overview

In the medical field, an ankle-foot orthosis (AFO) is a type of orthodic support designed to support the ankle in some way. This can be by helping to control the Ankle's position and motion during normal walking gain, compensating for a weakness of some kind in the foot, or to help correct deformities [2]. One common condition AFO's are used to treat is "Foot drop", a condition common among people who've suffered spinal cord or nervous system injuries, wherein the person experi-

ences an inability to lift their forefoot during walking [3], causing them to drag their toes along the ground. Many designs for ankle-foot orthoses (AFO) focus on either fully-active ankle actuation or on entirely restricting the motion of the foot itself. There are a number of different types of AFO designs out there, but more often than not the designs are often classified under the categories of conventional or solid ankle-foot orthoses (SAFO), or dynamically advanced ankle-foot orthoses(DAFO). [4].

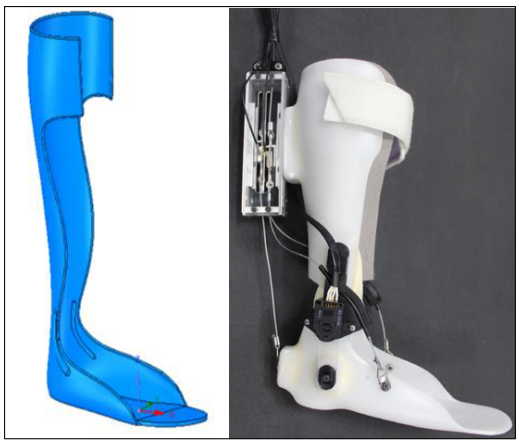

Figure 1.2: (Left) Example of a Solid Ankle-Foot Orthosis (SAFO) design[5]. Note that the entire design consists of a single component. (Right) Example of a powered Dynamic Ankle-Foot Orthosis (DAFO or pDAFO) design [6]. The bottom component is attached via a hinge-joint about the ankle and actuated via the load cell on the calf.

SAFOs are fully static devices designed to keep the user's foot locked at a fixed position. They are often made out of a single plastic cast, shaped to wrap around the user's leg. The SAFO developed by Chern JS, for example, is great at maintaining balance in the leg; however, the restrictions they place on the foot range of motion greatly affect ambulation [7]. Furthermore, being made out of one solid piece means that SAFO's are more susceptible to cracking due to stresses applied on the device during the stance phase [5]. All these faults meant that an SAFO design-scheme would be unsuitable for this type of project.

In contrast of SAFOs, DAFO devices consist of multiple components attached around an adjustable hinge-joint. This set-up helps to avoid restricting the total range of motion for the foot, and hence has less negative affects on total ambulation than standard SAFO devices. The adjustable hinge joint allows the walking angle to be modified for each user. This allows the device to help the user avoid foot drop, while still keeping the foot at a fixed angle during normal ambulation [4] [8]. This control over the ankle makes the DAFO design-scheme more suitable for this project than its counterpart. DAFO devices are also highly modifiable, with a wide arrange of options for controlling the operator's ankle. A review the literature shows that most DAFO devices can be classified as either passive, non-powered devices, actively-powered devices, or passively-powered devices [8].

1.2.2 Passively-Powered vs Actively-Powered AFOs

Powered DAFOs (PAFOs) are devices designed for the purpose of actuating the user's foot in some way so as to help control its position during the walking phase. These types of devices come in two varieties: Passively-Powered (pPAFO) and Actively Powered (aPAFO). Actively-Powered devices are just as they sound - DAFOs that implement electronically-powered devices, such as motors or actuators, in order to actively control the dorsiflexion and plantar-flexion motion of the ankle. One type of device utilizes a belt-chain mechanism attached to a DC motor in order to control both the dorsiflexion and plantarflexion motion of the ankle [4]. Another device also implemented a belt-chain system, but with a load cell modulator located at the back of the shank in order to move the ankle [6]. For both of these devices, the actuating component was located in the center of the leg, as placing it on either side would result in an uneven distribution of forces [4]. This is a key issue that occurs with PAFO's, in that the systems used to actuate the ankle joint are often

cumbersome, heaver, and can put unintended stresses on the operator's foot. Some designs try to get around these issues by simplifying the actuation system. The system designed by [9] relies on a servo motor at the ankle joint to control dorsiflexion and a controller to reduce total friction, rather than a complex belt-and-pulley system. A major problem with fully powered AFO devices, however, is that it is often difficult to 100 % align the motion of the user's foot using machines with normal human walking gait, due to the fact that this motion is typically initiated by the user's own leg [4]. Hence, it makes more sense for the AFO to supplement the pre-existing motion of the users' foot, rather than try to replace it entirely.

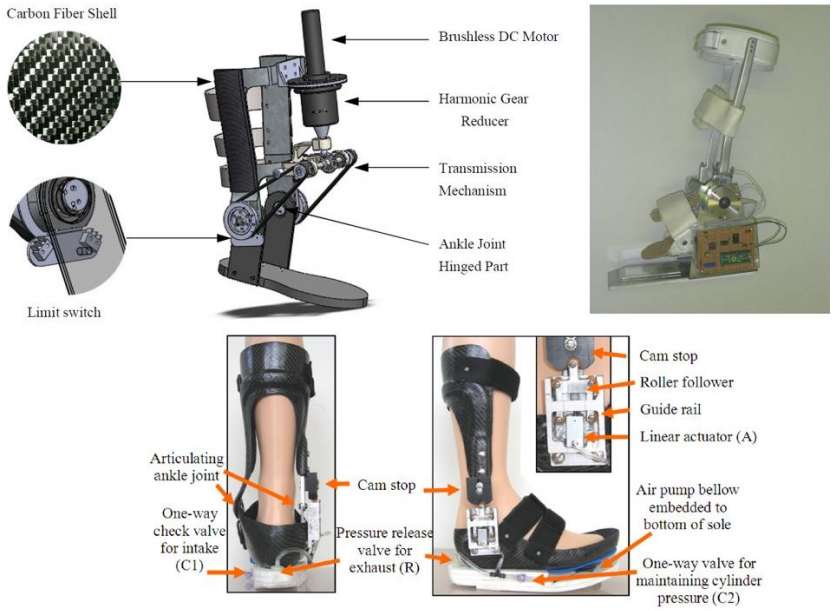

Figure 1.3: Various PAFO devices throughout the literature. (Top-Left) Active-PAFO (aPAFO) device that uses a motor-driven belt-chain set-up to control ankle tilt [4]; (Top-Right) aPAFO device that uses powered DC motor attached directly to the ankle-joint to control the wearer's foot [9]; (Bottom) passively-powered PAFO (pPAFO) device. When the user steps down, an air-pump attached to the bottom of the sole pushes air through a valve and into a linear actuator attached to the heel. The linear actuator, in turn, pulls against the sole, tilting it upwards and causes the foot to dorsiflex as a result.[10]

Like Active PAFOs, pPAFO devices can sometimes incorporate means of actu-

ating the operator's ankle. However, the amount of power provided is only enough to help control foot drop and dorsiflexion, not enough to fully drive the total motion of the ankle during normal walking. As such, pPAFOs are often worn by users who already have some way to move their legs. One such device even came up with a way to passively-power the foot swing motion using pneumatics, wherein an air-pump attached to the bottom of the sole would provide the power needed to provide dorsiflexion motion to the foot whenever touchdown occurred[10]. Another device developed by [11] utilized a myoelectric powered controller, wherein electrical signals from the controller are sent directly to the user's muscles, in order to actuate the ankle joint. Both methods provide means of controlling and actuating the user's ankle in order to avoid foot drop, without the need for expensive or cumbersome electronic motors or actuators.

1.2.3 Notable Devices

Throughout the literature, there were a couple of devices who happened to have a greater impact on the design of the AFO than others. One such design that had a major impact on both the AFO, as well as the design of the L.A.R.R.E exoskeleton as a whole, was the modular lower-limb exoskeleton system described within [12]. This particular exoskeleton had each joint designed to exist as their own separate subsystems, which could then be linked together via connection rods. These rods could have their overall length adjusted, allowing the exoskeleton to work with users of different heights. Additionally, each individual joint would be actively controlled via its own DC Servo motor. While the AFO described here did not incorporate the any active motors into its design, it did however incorporate the modularity design scheme used within this device to help it interface itself to the greater L.A.R.R.E system. Like [12], the AFO connects to the greater exoskeleton through two-rod

linkages with adjustable length jutting out of the top of the subsystem.

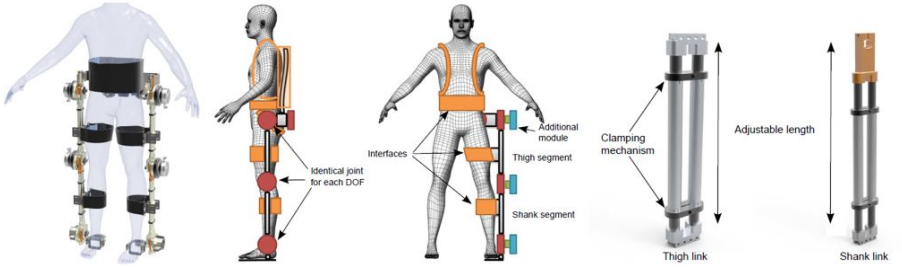

Figure 1.4: Modular-joint Exoskeleton design with adjustable linkages [12]

Another design that had a major influence on this project was the aPAFO developed by [13] due to its implementation of Force Sensing Resistor (FSR) sensors, embedded within the sole of the device. With a DC motor attached to the ankle-joint, the system was designed to help test new methods of controlling ankle actuation. In the device, the two FSRs embedded within the sole act as limit switches that control the actuation of the DC motor. As shown in figure 1.5, the FSRs were placed at select locations that correspond to the major pressure concentrations of the human foot: the Ball and the Heel. Depending which FSR is activated at any point in time, the device's onboard controller is able to determine what position the wearer's foot is in. In turn, the controller can then determine which specific transition stance within normal walking gait cycle the wearer's foot is currently in and, therefore, be able to adjust the DC motor accordingly.

The authors define the complete gait cycle by dividing it into five distinct gait events: heel strike (HS), flat foot (FF), heel off (HO), toe off (TO), and swing (S) [13]. Additionally, the paper also uses these gait events to define six transition events, of which the FSRs are used to help identify. The table used to categorize each of these transition phases in the paper is shown in table 1.1. This table, as well as the implementation of FSR sensors, played a huge role in influencing the design

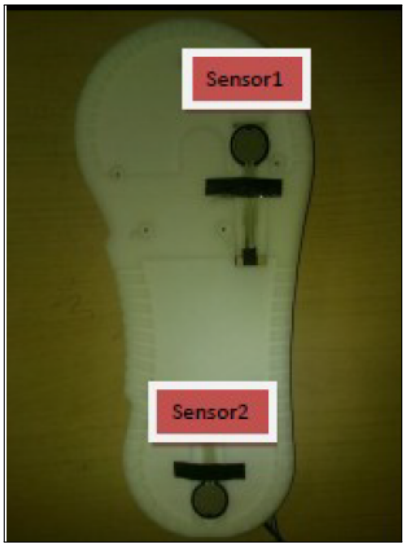

Figure 1.5: The sole of one powered DAFO device with Force Sensing Resistor sensors embedded inside. The FSRs allow the device to detect the different transition events that occur during normal walking gait [13].

of the Sole-Sensor discussed further within the paper. However, this device only used the FSRs as binary push-buttons, to detect the position of the AFO rather than the concentration of forces on the AFO itself.

Transitions in gait phase		FSR Sensor 1 (Ball)	FSR Sensor 2 (Heel)
T1	S - HS	OFF	ON
T2	HS - FF	ON	ON
T3	FF - HO	ON	OFF
T4	HO - TO	OFF	OFF
T5	TO - S	OFF	OFF
T6	HO - FF	ON	ON

Table 1.1: The Gait Phase Detection Algorithm table used within [13] to define which FSR-state combinations correspond to each transition phase within the normal walking gait cycle.

1.3 Research Contributions

Modular lower-limb exoskeletons such as the one described in [12] usually leave the ankle-joint component as little more than a small platform and strap to secure the foot with, providing little to no effort towards helping the ambulation movement of the user. Furthermore, while prior devices have experimented with both passively-powered dorsiflexion control and sensory feedback to detect foot position, there are not any devices that have combined these two aspects together into a single device. One feature that many of these devices have not attempted to incorporate, however, is the ability of the AFO device to detect the concentration of forces placed by the foot when in contact with the ground.

Unlike other devices listed throughout the literature, this device seeks to combine passive-dorsiflexion control methods and sensory feedback systems into a single AFO device that can both function on its own as well as serve as part of a greater lower-limb exoskeleton system. Detached from the greater exoskeleton, this device acts as a fully-functional DAFO device capable of controlling foot-drop using a passive torsional-spring system. When attached to the L.A.R.R.E, however, the device is able to provide real-time sensory input to the exoskeleton telling it the current ankle-orientation and whether the foot is in contact with the ground, helping it maintain balance. Important to the task of maintaining balance in Humanoid robots, however, is the ability to track the distribution of forces placed on the foot when in contact with the ground. This is where the main contribution of this particular device of this device comes in. While other AFOs in the literature have shown that integrating FSR sensors embedded within the sole can be used to detect the position of the user's ankle, this device serves to show that this same set-up can also be used to determine the distribution of forces placed by the user's foot on the device. By using

three FSRs instead of two, it becomes possible to determine the Center-of-Pressure point within the support polygon they form. This information can then be used by the main controller on-board the L.A.R.R.E to help the system maintain its balance.

Chapter 2

Mechanical Design

This section discusses the overall thought process and work that went into the mechanical design of the AFO. There mechanical design of the AFO was designed to satisfy four main goals: 1) To provide passive dorsiflexion support to the operator's foot; 2) To support the combined weight of both the operator and the other portions of the L.A.R.R.E system; 3) Entire system must weight under 2lbs; 4) To provide real-time force-concentration location and foot-position information from sensors embedded within the sole. In order to achieve dorsiflexion support, a torsional spring was placed around the ankle joint and connected to both halves of the system. The spring automatically returns to its default position after being stretched, allowing the AFO to help control the position of the operator's foot without any electrical power. To maintain the weight of both the operator and the exoskeleton, the joint-axle component was itself made out of alloy steel to make it as sturdy as possible. In contrast, the rest of the metal components were made using Aluminum in order to keep the AFO relatively lightweight, such as with the footplate component. The Footplate itself contains a small cavity inside of it in order to hold the custom "Force-Sensing Foot-Sole" sensor discussed within Chapter 3.

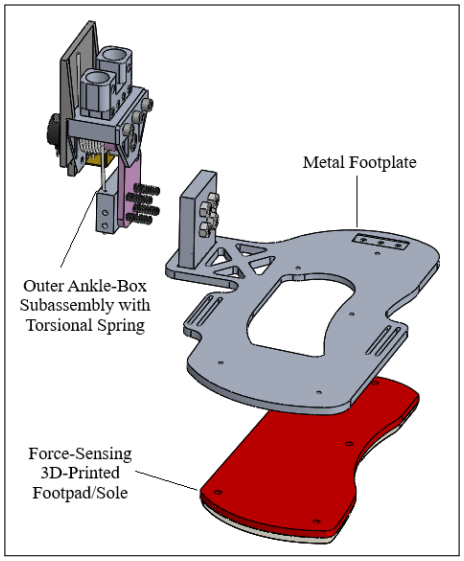

Figure 2.1: AFO Frame and Sensor Design

2.1 AFO Design Requirements Overview

2.1.1 Requirement 1) Passive Dorsiflexion Control

To fulfill its role as an Ankle-Foot Orthosis and help the L.A.R.R.E in its role of medical rehabilitation, the device must be able to provide some form of assistance to the operator's ankle. One of the most basic forms of assistance that AFO devices provide is reduction of the effects of foot-drop, wherein a lack of muscle control causes a person to drag their foot across the ground as they walk [3]. In the case of the L.A.R.R.E, ambulation will be driven by DC motors attached to the Hip Joints, as well as Electrical-Muscle Stimulation (EMS) applied directly to the operator's leg muscles. Hence, the reason why the Ankle-Joint is unpowered. However, while these methods will help the operator walk while wearing the exoskeleton, they will not by themselves be enough to stop the operator's foot from dragging across the ground.

To control for foot-drop, the Ankle-Joint must include some system to passively

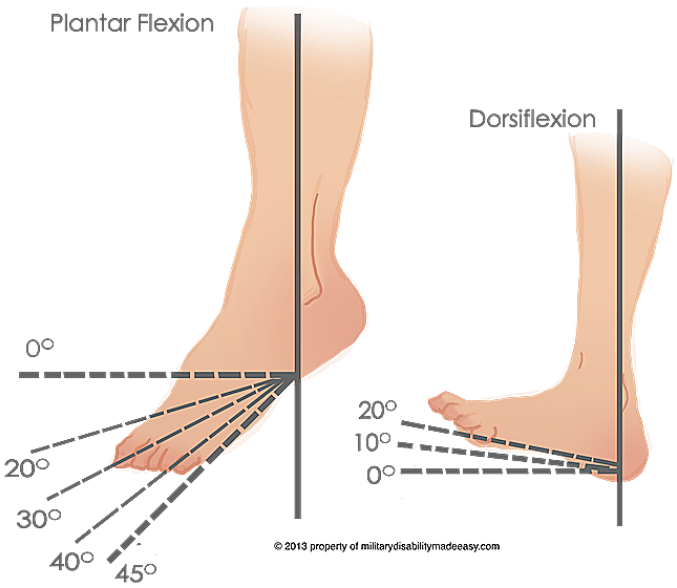

Figure 2.2: Dorsiflexion and Plantar Flexion Range-of-Motion [14]

adjust the operator's ankle. If their feet start to drag, the AFO should be able to pull both their foot back into the standard flat-foot position. As this would be a mostly upward motion, the AFO would technically be helping the operator Dorsiflex. Dorsiflexion is the act of tilting one's foot such that the toes point towards the shins [1]. For an average human adult, the typical Dorsiflexion range is between 0°-to-20°[14], as can be seen in Figure 2.2.

2.1.2 Requirement 2) Support Load from Exoskeleton

As the majority of the Sub-Systems and Mechanical components that will make up L.A.R.R.E will be placed directly above the Ankle-Joint, it only makes sense that the AFO should be able to handle the load placed on it by the Exoskeleton without breaking. Hence, the Ankle-Joint Axle/Shaft component, of which the Footplate sub-system rotates about and which the entire load of the Exoskeleton is placed on, must be as structurally strong as possible. For if this particular part should happen to break while someone is operating L.A.R.R.E, then the operator would suddenly

find themselves supporting the entire weight of the Exoskeleton with their body as opposed to the other way around. This in turn would cause the L.A.R.R.E to be unable to keep itself upright and fall over, which could seriously injure the operator.

2.1.3 Requirement 3) Weigh as close to 2lbs as possible

In order to reduce the total amount of work the user's muscles would have to put out in order to walk, as well as the amount of torque needed to passively control the user's ankle, the individual components that make up the device were designed to be as lightweight as possible. This is especially true with the Metal Footplate component, the largest component of the AFO and also the most massive. Hence, the reason why this component has a large cavity cut out of its center - to reduce its total mass. Early on in development, it was decided that the total AFO system should weight as close to 2lbs as possible in order not to negatively impact the performance of L.A.R.R.E.

2.1.4 Requirement 4) Real-Time Foot-Position and Force-Concentration Feedback

In order for the L.A.R.R.E to properly maintain its balance during normal walking gait, it needs to be able to accurately calculate its Center-of-Mass. In order to find the Center-of-Mass in real-time, the Ankle-Joint Systems need to be able to provide information regarding both the current position of the Ankle-Joint, whether or not the Footplate is in contact with the ground, and where the Concentration of Forces placed on the Footplate are located. It is for these reasons why the Force-Sensing Sole-Sensor, described in greater depth in Chapter 3, was developed. It is also for this reason why a Potentiometer is attached directly to the Ankle-Joint's Axle/Shaft

component, so as to verify the angular position of the Ankle even when the footplate is lifted off the ground in mid-swing.

2.2 Outer Ankle-Box Subsystem

The sub-assembly known as the "Outer Ankle-Box" acts as the main ankle joint for the AFO, connecting the Footplate Subsystem to the rest of the LARRE Exoskeleton. It contains the ankle joint axle, the torsional spring for dorsiflexion control, and the potentiometer used for measuring the angle of deflection, as shown in figure 2.3. The torsional spring is held in place around the axle via two holes drilled into the "End Cap Coupler" and "Spring Holder Block" components, which hold the two ends of the spring in place. The "Shank Arm" binds to the axle through a spring pin, and helps transfer load directly through to the footplate itself. It does this due to the design of the collet that surrounds the shaft. Originally, the shank arm as designed to connect to the axle through the use of a key-shaft. This was later changed to using a spring-pin to connect the two components together, once it was learned how difficult manufacturing a proper key-channel into the collet would be. The ankle joint axle has a small cavity carved within one end in order to allow the potentiometer shaft to fit inside it.

2.2.1 Providing necessary torque for Dorsiflexion

In order for the AFO to provide adequate dorsiflexion support, the Torsional spring must have enough torque to pull the operator's foot back into the default "flat" position. As this system is designed to be for general use, rather than for any one specific individual, several assumptions about the operator had to be made during the design process. For example, the average adult human male has a a total mass

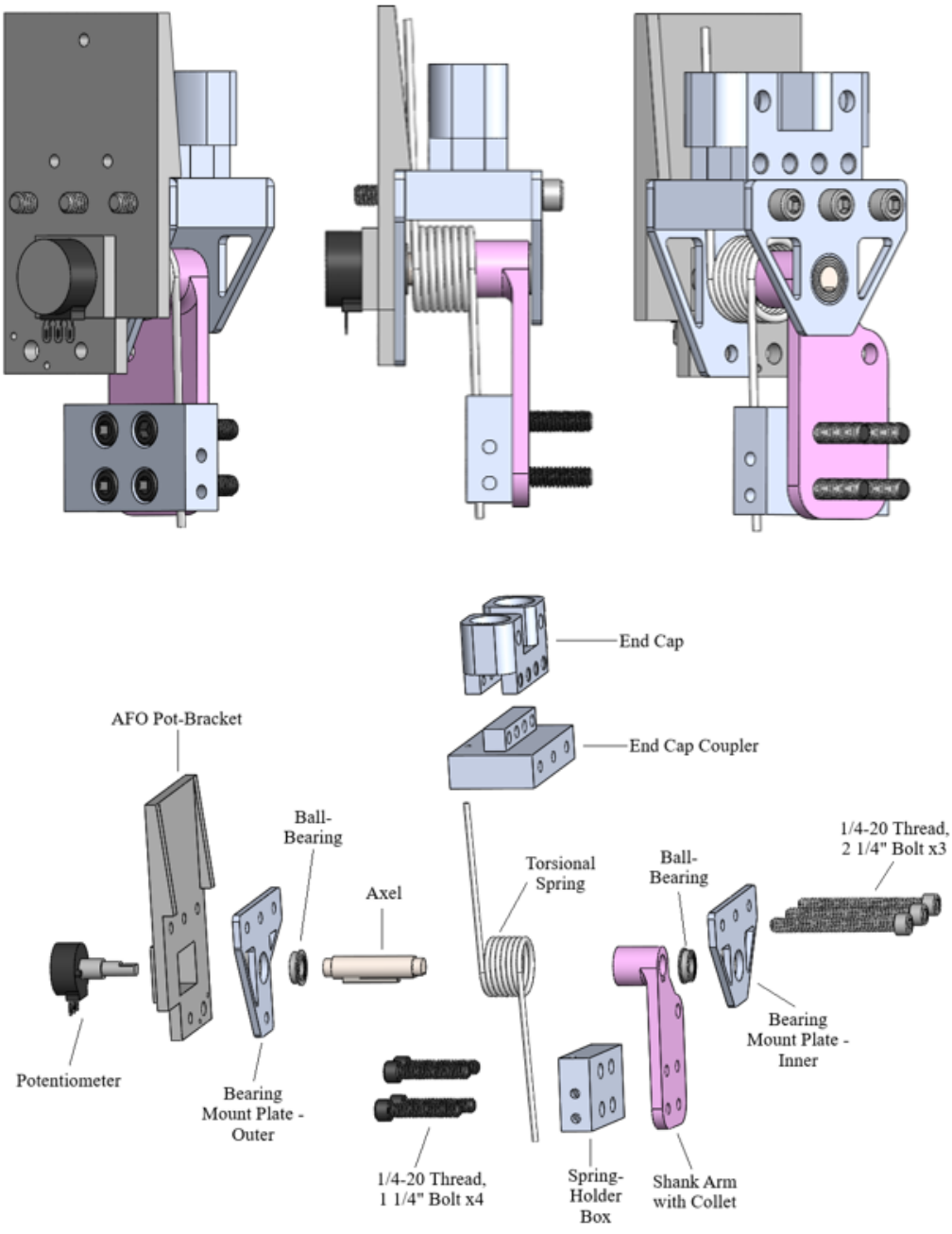

Figure 2.3: (Top) Multiple views of the complete "Outer Ankle-Box" sub-assembly. (Bottom) Exploded View of the "Outer Ankle-Box" Mechanical Subsystem, with all individual components labeled.

of approximately 65kg. Using estimates of both the user's foot mass and Center-of-mass location taken from [15], where estimate foot mass is $m_f = 0.91kg$ and Foot

CoM location is $l_{COM} = 0.139m$, it was possible to calculate the required minimum torque needed to dorsiflex the users foot. This was calculated using Eqn 2.1 to be $\tau_foot = 1.24N * m = 10.98lbsf * in$, where $g = 9.81m/s^2$ is gravitational acceleration.

$$\tau_{foot} = l_{COM_f}(m_f + m_e)g \tag{2.1}$$

However, as the spring would have to account for the mass of both the foot and the AFO system together, it was also necessary to calculate the torque needed to move the AFO component by itself. As the rest of AFO had not been fully designed yet at this stage of development, the mass of the AFO footplate was estimated to be $m_{estAFO} = 0.5kg$, and the Center-of-Mass location was estimated to be $l_{COM_{est}} = 0.1m$ away from the ankle joint. By plugging these values into Eqn 2.2, the the necessary torque needed to move the estimated AFO by itself was found to be $\tau_est = 0.49N * m$.

$$\tau_{est} = l_{COM_{EXO}} m_{EXO_{est}} g \tag{2.2}$$

Finally, by combining the values of Foot Torque τ_{foot} and Estimated AFO Torque τ_{est}, as seen in 2.3, the minimum torque needed to move both the foot and the AFO together is $\tau_{total} = 1.73N * m = 15.311lbs * in$. Knowing this, a torsional spring with a rated spring load of $17LbsIn$ was chosen for the design, the CAD model of which is shown in Figure 2.4.

$$\tau_{total} = \tau_{foot} + \tau_{est} \tag{2.3}$$

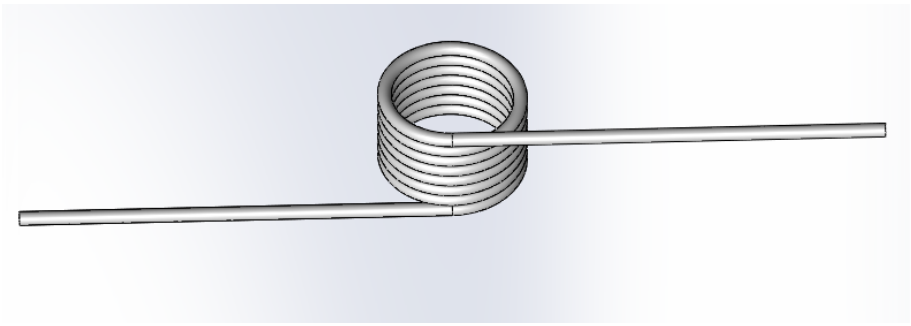

Figure 2.4: CAD Model of the Torsional Spring product used within this design.

2.2.2 Load Transfer through Ankle Joint

Within the greater L.A.R.R.E system, the main job of the AFO is to support the combined static weight load of both the rest of the exoskeleton, as well as that of the human operator, without buckling. As such, the Outer-Ankle Box sub-system needs to be redistribute all the load placed on it through the ankle-joint and into the Footplates. All of these components must be strong enough to hold up some desired maximum load, which in this case is the weight of the user multiplied by some determined factor of safety (FoS), as described in equation 2.4. The factor of safety number takes into account the extra stress placed on the component due to the weight of the rest of the exoskeleton. In this case, the Factor of Safety was set as 5 in order to overcompensate for the eventual, unknown final mass of the exoskeleton. According to [15], the average mass of an adult human male in North America is around $73kg$. Using this number as the expected mass of the human operator, and multiplying that number by the acceleration due to gravity $g = 9.81m/s^2$, the amount of force applied this applies on the Outer-Ankle Box would be close to $716.13N$. Multiply that by a Safety Factor of 5, and the force that the joint axle needs to be able to support is at least $3,580N$.

$$F_{Load_{MIN}} = (m_{user} \cdot g) \cdot FoS \tag{2.4}$$

All the load first acts on the Joint Assembly through the top tab of the "End Cap-Coupler" component, as listed within Figure 2.3. This in turn is transferred through two "Bearing Mounting Plates", through ball-bearings and into the Ankle Joint Axle/Shaft component. The load is then transferred from the axle into the component known as the "Shank Arm with Collet", which in turn transfers the load into the Footplate through the "Ankle-Mounting Plate" component. A full Force-Body diagram showing the distribution of forces through the ankle-joint is shown below in figure 2.5.

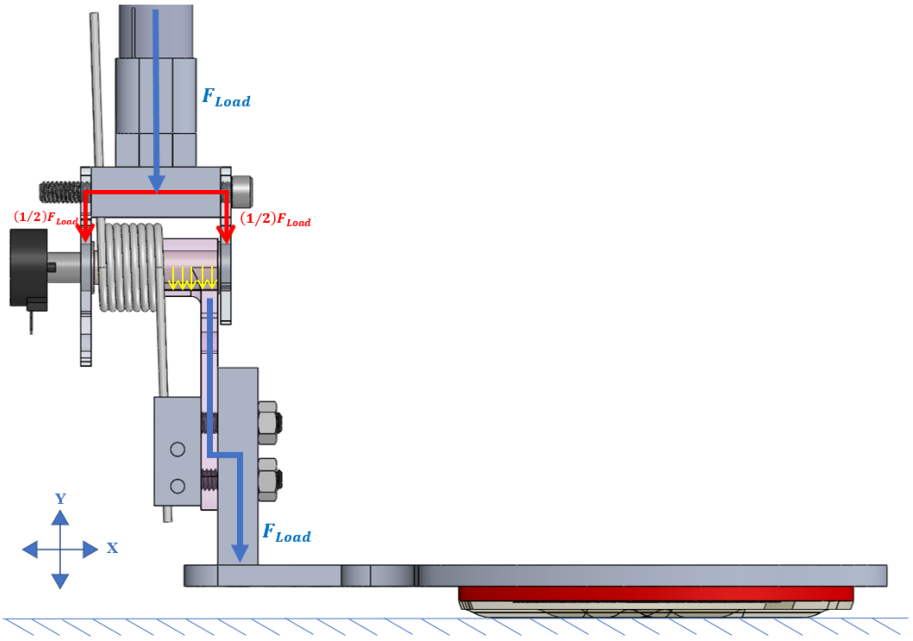

Figure 2.5: Force-Body Diagram showing distribution of the load from the exoskeleton through the ankle joint and into the Footplate.

End-Cap Coupler Overview

The End-Cap Coupler, also known as the Coupler, is designed to connect the AFO sub-system with the rest of the L.A.R.R.E Exoskeleton. As shown within Figure 2.6, the component takes the form of a rectangular body with a thin-tab jutting out

from the top with a height of $10mm$. This tab contains four $5.5mm$ diameter holes, used to interface directly with the "End-Cap" component that's used throughout the L.A.R.R.E exoskeleton. All the load from the rest of the exoskeleton, shown as F_L in Figure 2.5, is transferred through the End-Cap and into the Coupler through this tab. This load is in turn transferred into the Axle from the Coupler through the two Bearing Mount plates, which connect to Coupler through three $1/4" - 20$ threaded holes located on both sides of the larger rectangular section. In addition to transferring load, the End-Cap Coupler also serves to help affix the torsional spring in place around the shaft. On one side of the Coupler, a small hole with a diameter of around 0.3" is drilled between the threaded screw holes. As the end of the wire that makes up the torsional spring has a cross-section diameter of 0.298", this opening creates a snug fit that holds one end of the spring in place.

Ankle-Joint Axle Overview

The purpose of this component is to transfer that load to the Footplate through the Shank-Arm component, while still allowing the subsystem to rotate about the joint. Additionally, the joint-axle also has a small cavity drilled into one side of the shaft, as shown in figure 2.6, in order to allow the potentiometer's shaft to fit inside and connect directly to the axle. Hence, it was absolutely imperative during the design process that the ankle joint be able to handle all these tasks without failing. It is for these reasons why the axle-joint component is manufactured out of steel, rather than Aluminum like the rest of the components. Additionally, this component also went through extensive FEA static load simulations in order to ensure the geometry would not result in any major stress concentrations. The results of these tests can be found in Section 4.1 of the paper.

Originally, this was designed to interface with the "Shank Arm with Collet"

component, also known as the Shank-Arm, through the use of a square key-shaft component. This can still be seen in the geometry of the channels seen within both components, which were made using the end-tips of a CNC machine. At the time, it was assumed that the rounded edges of said channels would be cut-through using a key-shaft cutting tool, in order to allow the key to actually fit inside the channel. However, only became apparent after most of the manufacturing was done that the key-shaft cutting tool could not fit within the opening of the Shank-Arm, and as such could not complete the square channel. Hence, it was then decided to instead use a spring-pin to connect the two components together in place of the key-shaft. This required manually drilling holes into the sides of both components to allow the spring-pin to fit through, which do not appear in the CAD models. Like the Axle component, the spring pin is made out of stainless steel, increasing its overall structural strength.

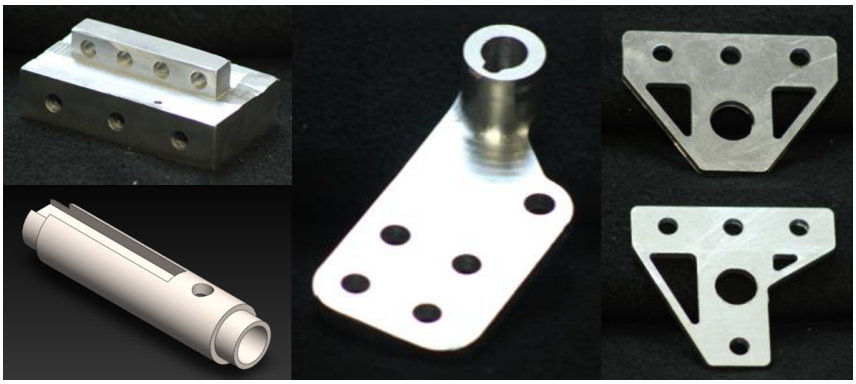

Figure 2.6: Main components within the Outer-Ankle Box Sub-assembly that transfer the load from the L.A.R.R.E. Exoskeleton through to the Footplate. (Top-Left) End-Cap Coupler; (Bottom-Left) Ankle Joint Axle Shaft; (Middle) Shank-Arm with Collet; (Top-Right) Inner-Bearing Mount Plate; (Bottom-Right) Outer-Bearing Mount Plate;

Shank-Arm with Collet Overview

The "Shank-Arm with Collet" component is what connects the Ankle-Joint Axle directly to the Footplate sub-system. It has a small "collet" shape that wraps around the geometry of the axle while still being small enough to not come into contact with the torsional spring, which can be seen in figure 2.6. A $5mm$ thin plate-like extrusion juts down from the collet. This extrusion contains four 1/4" Diameter Tapped holes, used for mounting the "Shank Arm with Collet" component to both the "Spring Box" and "Ankle-Mounting Plate" components. As the load from the rest of the exoskeleton is transferred from the axle shaft through the collet and into the extrusion, its imperative that the component not break under the load. To address this, a small fillet was placed around the area between the extrusion-arm and the collet, in order to reduce potential stress concentrations.

As mentioned before, it has a small channel cut into one end of the shaft-opening in order to allow it to interface with the Axle through a key-shaft. However, due to manufacturing issues, the role of the keyshaft is replaced with a spring pin pushed through holes drilled on the sides of the collet. Another feature cut from the design was the inclusion of a small, safety-stop button that would of affixed the Shank Arm in place by pushing a small rod through a hole located on the component. This small sub-system would have connected to the Outer-Ankle Box from the outer edge, and would fit within the gap provided by the Outer Bearing Mounting Plate component. This sub-assembly was later scrapped during the manufacturing phase as it was determined to be a non-essential system. However, evidence of this system can still be seen in the $5th$ hole located to the side of the collet.

Bearing Mounting Plates Overview

The "Bearing Mounting Plates" connect the End-Cap coupler directly to ball-bearings attached to the axle shaft. Each plate is made out of 1/8" thick, 6061 $T6$ Aluminum plates. They connect to the End-Cap Coupler component through the three mounting holes, made to allow $1/4" - 20$ Threaded screws to go through and screw into the End-Cap Coupler in place. and a larger hole towards the bottom for holding the ball bearing component. As the amount of load placed on the End-Cap Coupler is halved through each plate, these components can afford to be thinner than the other components. The strength of these components are proved within the FEA Static Load Simulations described in Chapter 4.

As can be seen in Figures 2.3 and 2.6, two separate designs for the Bearing Mounting plates are used within this system. This is because the outside facing edge of the Outer-Ankle Box has additional features that the inner facing edge does not, such as the potentiometer and the Pot Mounting bracket. As such, the Bearing Mounting plate on the outermost-facing side needed to be designed around these features. Additionally, the The canceled "Safety-button" sub-system described earlier had a profound affect on the design

2.3 Footplate Subsystem

The main role of the Footplate subsystem is to provide a platform for the user to stand on that secures their foot into place, while also providing a form of housing for the Sole-Sensor and other components. The Footplate subsystem consists of three main components: the metal Footplate-component itself, the "Ankle Mounting Plate" component that connects the footplate to the Outer-Ankle Box sub-assembly, and the Force Sensing Foot-Sole or "Sole-Sensor" discussed in length in Chapter

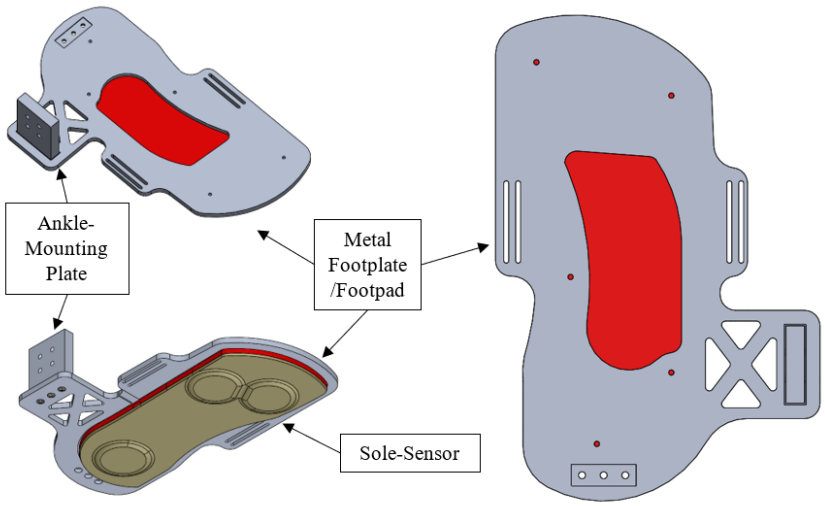

Figure 2.7: Basic overview of the "Footplate" subsystem of the AFO. The Force-Sensing "Sole-Sensor" is installed at the bottom of the metal footplate component allows the AFO to detect the distribution of forces placed by the foot.

3. Both of the metal components were manufactured out of 6061 $T6$ Aluminum Alloy plates, whereas the Sole-Sensor was made using a combination of 3D-printed material and Vytaflex-20 polyurethane rubber. These materials were chosen in order to keep the overall mass of the Footplate subsystem as close to $0.5kg$ as possible, as any additional mass would reduce the ability of the torsional spring to control dorsiflexion motion, not to mention place additional strain on the exoskeleton's operator.

The Footplate itself is designed to be large enough to encompass the user's shoe, being over 12" long and 8" wide. Small slits located at the sides allow the use of a Velcro strap in order to affix the user's shoe to the component. The Sole-Sensor is designed to be installed within the Footplate through the use of the five screw holes located at the top of the component, fitting itself within the small cavity located at the bottom. All these features can be seen within figure 2.8.

Towards the heel is a small slot with $3\ 1/4" - 20$ Mounting holes. The purpose of this slot is to help future proof the design, by allowing the possibility of additional

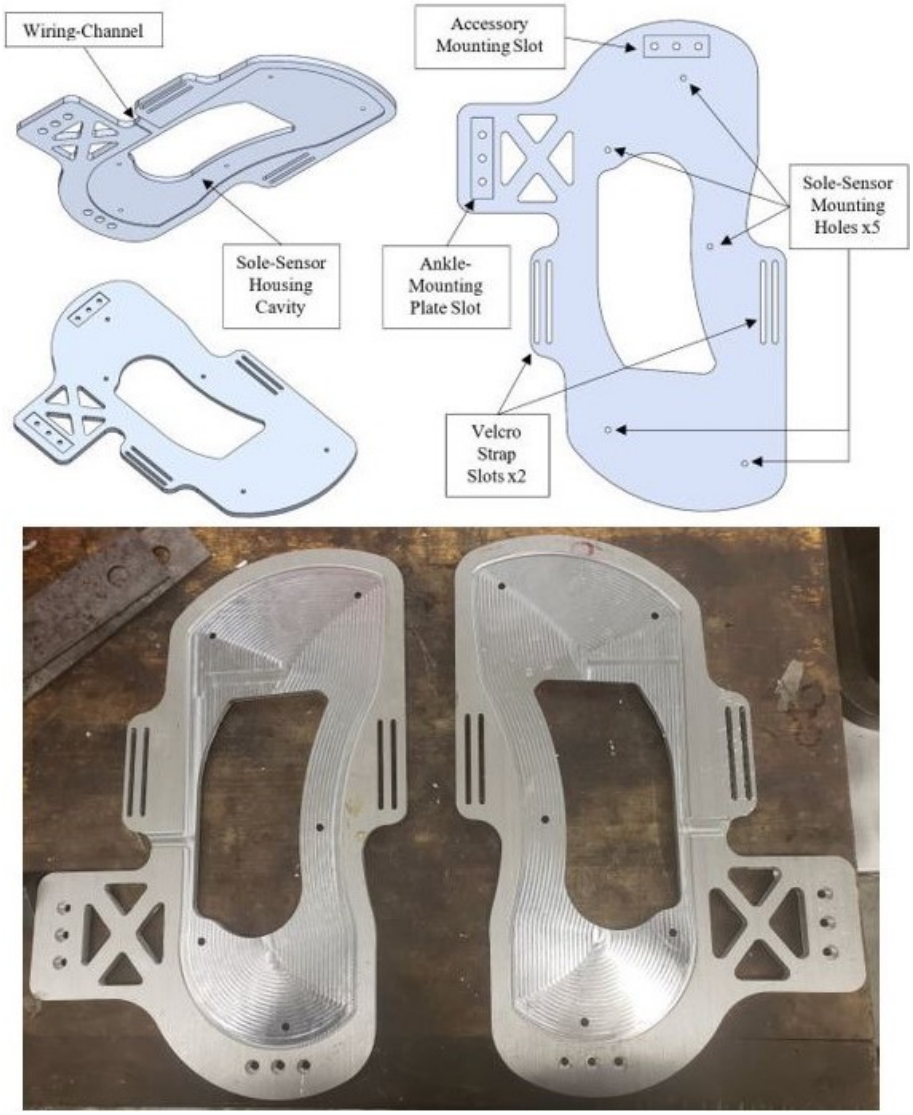

Figure 2.8: (Top) Multiple views of the Metal Footplate component, displaying each of the main features within the design. (Bottom) Both the Left and Right Footplate components flipped upside-down immediately after manufacturing. The thin cavity where the Sole-Sensor is installed is clearly visible, as are the marks made my the end-mill used to carve it out.

accessories that can be attached to the footplate. One such accessory was the MOCAP-marker Horseshoe component, used within the Sole-Sensor tests described within Chapter 3. This component is designed to wrap itself around the footplate, such that the same straps used secure the operator's foot in place also secure it to

the footplate. The Horseshoe has spots to house three VICOM MOCAP Markers at specified locations around the Footplate. These Markers are then used to help measure and track the Center-of-Pressure location of the AFO, as explained further in Chapter 4.

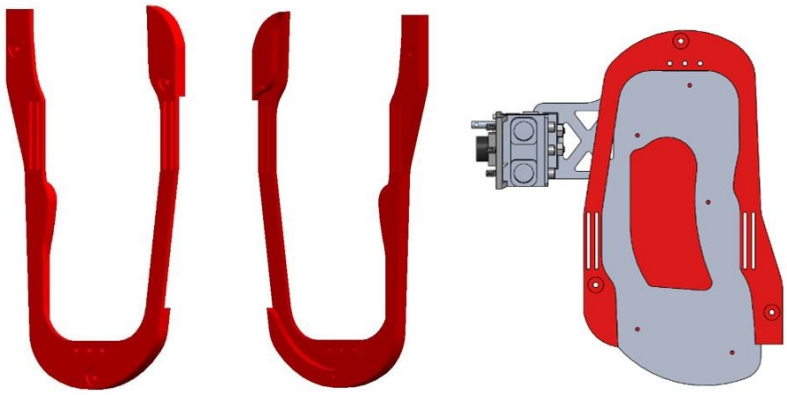

Figure 2.9: CAD Rendering of the MOCAP Horseshoe Component attaching to the footplate.

Chapter 3

Force-Sensing Foot Sole

This chapter discusses the methodology and the choices behind the development of the force-sensing foot sole components. The Force Sensing Footsole, or "sole-sensor", is a specialized sensor component embedded into the main footplate of the AFO, designed for the purpose of determining when the user's foot is in contact with the ground, what position the foot is in at any given moment, and how the foot transitions from the Toe-Down to Heel-Down positions. It is able to achieve this through the use of Force-Sensing Resistor (FSR) sensors that allow the system to determine the location on the footpad where the user's foot is exerting the most force. The Footsole itself consists of three Force-Sensing Resistors (FSRs), placed at select locations on a 3D-printed "footpad" piece, encased within a Vytaflex-20 Polyurethane rubber resin cast for protection. This set-up allows the footsole to accurately detect not just when the user is stepping down, but also what position their foot is in at a given moment depending on the FSR readings. Furthermore, the use of a rubber coating along the bottom of the sole allows the sensor to properly "grip" the ground, allowing the user to walk while wearing the AFO without accidentally slipping.

3.1 Electronics Overview

3.1.1 FSR Component Overview and Circuit Set-Up

By definition, FSRs are any type of material whose internal resistance changes when a force or pressure is applied to it[16]. The internal resistance changes in response to external loads at an average rate of 3Hz, though the measured resistance often falls within a certain range rather than a specific value for a set load. This property makes such devices useful for detecting when a weight is being applied, though not so useful for detecting the exact amount of weight. The specific FSRs used in this design, Ohmite FSR03C3, consists of a flat, circular area with two pins jutting out from it, as shown in figure 3.1. The default internal resistance for these devices rests at 0Ω when no force or pressure is applied. When activated, however, the internal resistance can jump upwards to as much as $10M\Omega$, depending on the amount of force applied to the sensor[17].

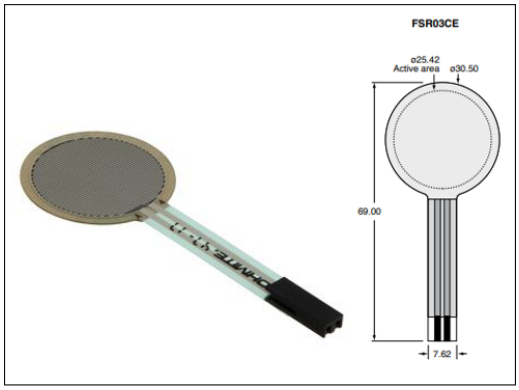

Figure 3.1: The Force Sensing Resistor Component (FSR03CE) used within the Sole-Sensor [17].

In order to allow a board to interpret changes within the FSR's internal resistance into readable data, the internal-resistance changes need to be converted into analog data signals. This is done by connecting one FSR pin to the board's power, and

the other pin connected to a pull-down resistor, as is seen in figure 3.2. This simple circuit converts the resistance readings into analog values lying within a range from $0 - to - 1023$, depending on the amount of force applied.

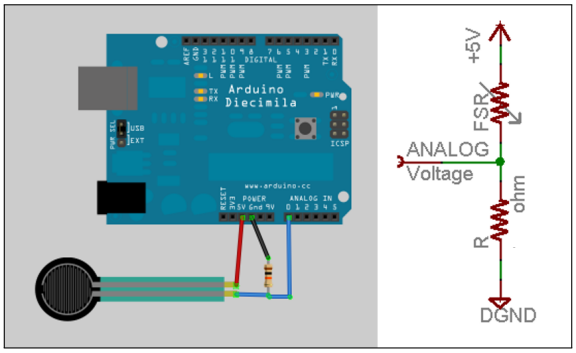

Figure 3.2: Circuit Set-Up for converting changes in FSR resistances to digital readings using a pull-down resistor [18]

The analog value for a given force can vary greatly depending on resistance of the pull-down resistor that's used within this kind of circuit. Having the ability to adjust the incoming values is crucial to making the sole-sensor work properly, especially when taking into account the effect that the resin would have on the default resistance readings. This was tested early on by a single FSR within a $5mm$ thick bit of resin and reading their default resistances. The results showed that the resin increased the default analog values from 0 to as much as 500, depending on the type of rubber. Changing out the pull-down resistor used, however, was found to either reduce or greatly increase the sensitivity to the resin. Lower resistances, such as those in the 100Ω range were found to greatly reduce the overall sensitivity to the resin, such that the "default" FSR values were brought from 750 to as low as 50. In contrast, higher resistances in the $100k\Omega$ range greatly increased sensitivity such that the default readings were close to the maximum 1023 value. After a bit of trial and error, it was decided that 150Ω would work well for the role of the pull-down resistor. This resistance helps keep the values returned by the resin-encased FSRs

at 0 when no load is applied, but also allows a wide arrange of values to be returned, from 200 up to around 900, depending on the magnitude of the load applied.

3.1.2 Sole-Sensor Circuit

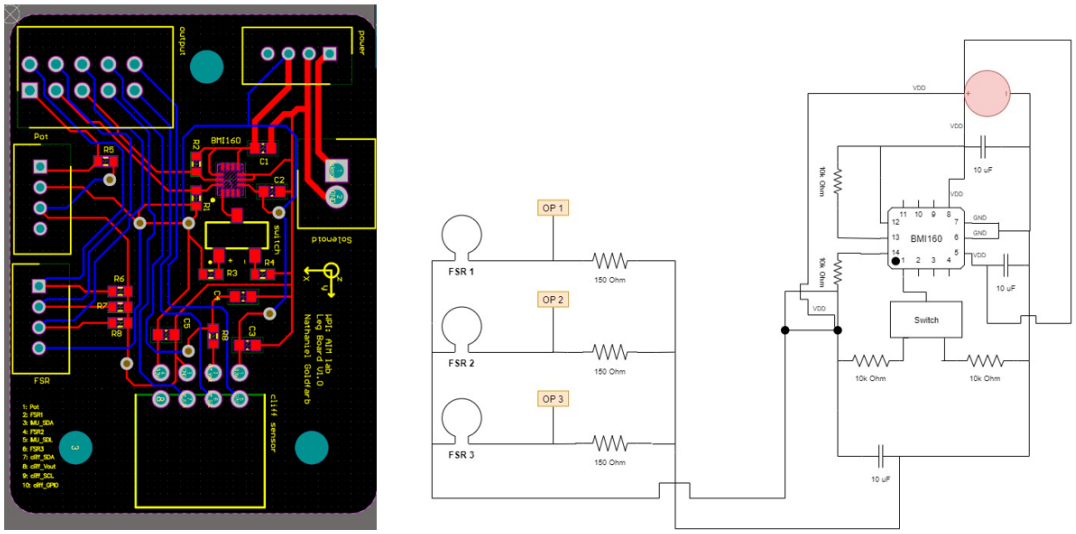

Figure 3.3: (Left) Layout of the actual circuit board used for reading sensor data throughout the L.A.R.R.E (Right) Detailed Diagram of how the 3 FSRs in the sole-sensor connect the the rest of the Board

Embedded within each Sole-Sensor units are three individual FSR sensors. Each FSR has one dedicated to as the INPUT-READ pin, with the other being used as the GROUND pin. The wires for each GND pin are soldered together into a single wire, in order to ensure that each sensor is being connected to the same GND source and received consistent readings. The four wires are then installed inside a crimp-connector, which can then be plugged into the main Sensor-Reading circuit board designed by the WPI AIM Lab, shown on the left-side of figure 3.3.

Throughout the L.A.R.R.E system, the same type of custom-made circuit board is used in order to read and process incoming sensor data. These boards contain built-in IMU sensors, in addition to input ports to read in data from other types of

sensors. Within the AFO, this board is used to read-in incoming data from both the Sole-Sensor, and the potentiometer attached to the ankle-axle. Each circuit uses pull down resistors of the decided 150Ω resistance in order to read the incoming FSR data from the designated "FSR Connection" port. Within the board, each FSR has its own individual pull-down resistor for reading in data, but all three are connected to the same GROUND pin. This set up allows us to get consistent readings from each FSR, while also avoiding having those same readings interfere with one another when multiple FSRs are activated together. A complete map isolating the FSR-pin connections within the board to the main power-source is given in the right-side of figure 3.3. This isolated map was crucial in helping to identify potential sensor-reading errors within the 1st iteration of the Sole-Sensor, as discussed in much greater detail in section 3.3.1.

3.2 Rubber Resin Selection and Molding

3.2.1 Resin Coating Overview

The rubber coating at the bottom of the foot-sole serves two main roles: 1) It acts as a protective layer that shields the millimeter-thin FSR sensors from damage due to repeated contact with the ground; and 2) It provides a rough, non-slippery surface to the footsole such that the static friction between it and the ground inhibits slipping during normal walking. This is especially important for the exoskeleton, as the system needs to be able to keep itself stable at all times. Two different types of polyurethane rubbers were considered for this role: Vytaflex-20 and Vytaflex-30. These materials were considered because of they form relatively stiff and non-pliable resin structures when cured, as shown in the material properties table in 3.1. This is the reason why other commonly used resin materials such as Dragonflex and Ecoflex,

were not considered for this project, as they work better for forming molds around preset geometry as opposed to forming new components.

In order to know which one of these materials would work best, we looked for the following properties: 1) How smooth or rough the texture of these rubbers are once fully cured; 2) How does the same amount of each type of resin affect the resolution of values returned via the FSRs? and 3) What affect, if any, does the addition of the resin material have on the amount of time it takes for the FSRs to react to any forces applied on them. For these tests, a small test-mold was made using 3D-printing. This test mold consisted of two components: a flat "bed" component, where the FSR would be placed, and the Mold-shell covering itself. The Mold-Shell has a small opening at the top to allow the resin material to be poured in. The resulting text-assemblies, for both Vytaflex-20 and Vytaflex-30, can be seen below in figure 3.4.

Figure 3.4: Two FSR sensors encased within two different types of Polyurethane rubber resins. (Left) Vytaflex-20 (Right) Vytaflex-30

The results of the FSR aspects are discussed in section 3.1.1, but to summarize there was no noticeable difference in terms of how each resin affected the resolution of values returned by the FSRs. While encasing the FSRs in resin did have an affect on the range of values returned compared to not being encased, this change was

observed to be equivalent regardless of what resin material was used. Despite the FSR results, there was a noticeable difference in the texture and consistency of the two materials once fully cured.

Material	Specific Volume	Color	Shore A Hardness	Tensile Strength
Vytaflex-20	27.7	Clear Amber	$20A$	200 psi
Vytaflex-30	27.3	Off-White	$30A$	500 psi

Table 3.1: Resin Material Properties Comparison Table

As shown in Table 3.1 [19], the Vytaflex-30 has both a greater Tensile Strength and Shore Hardness factors than the Vytaflex-20. In theory, these properties by themselves would make Vytaflex-30 more suitable for this kind of application. However, it was found that once cured the Vytaflex-30 material has a smooth and somewhat sticky surface texture. This is an unfortunate property to have for a material meant to act as a foot sole, as the smooth texture could result in the user's foot slipping when strapped to the device. In contrast, cured Vytaflex-20 has a much rougher texture, making it better for preventing slippage than its counterpart. Its for this reason why Vytaflex-20 was chosen as the material to form the rubber mold of the sole over Vytaflex-30.

3.2.2 Molding Procedure

When shipped, the rubber material arrives as two separate liquid-like materials: The resin itself and the curing catalyst. In order to use the rubber within molds, one must mix an equal volume of both the resin and catalyst materials together. Upon contact with the liquid resin, the catalyst material will immediately start the chemical curing process that turns the liquid rubber solid. Before the mixture turns solid, however, there is still a certain amount of time wherein the mixture remains viscous enough such that it can be poured into the desired mold without issue. This

property is called the POT LIFE, which for the Vytaflex 20 material is 30 minutes after first contact with the catalyst.

Before pouring the mixture into the mold, however, if first has to go through a vacuum chamber to remove trapped air bubbles from the material. While mixing the resin and catalyst materials together, small pockets of air will get trapped inside the mixture as air bubbles. This outcome is unavoidable, as not mixing these materials properly will result in an improper curing. These air are usually small, and only become noticeable once with mixture finishes curing. If not removed, the air bubbles can affect how the resin distributes forces applied to it in an unpredictable manner. To remove these air bubbles, the resin mixture must be placed within an air-tight vacuum chamber immediately once the mixing process is finished. By sucking out all the air inside the pressure, the internal ambient pressure is reduced until it becomes lower than the vapor pressure of the liquid resin. This low pressure soon causes the air bubble trapped within the resin to rapidly rise up and escape. This process similar to how opening a soda bottle causes the drink to fizz up due to the sudden change in air pressure, and in fact the resin material itself will start to resemble soda fizz due to the amount of air trying to escape it at once forming massive bubbles. Once the resin material starts to bubble up, it can remain in this phase for around $3-6$ minutes, depending on the amount of air trapped inside it. Once the majority of the air has been released, however, these bubbles will start to rapidly collapse until the majority of the resin returns to a homogeneous liquid form. Some excess air bubbles may still exist within the resin after the stage, though spending a few more minutes in the air chamber can remove most of these as well.

Considering that the resin material starts losing its viscosity around $26-30$ minutes after combining with the catalyst, it is absolutely imperative that the user keep careful track of the passage of time for both mixing the material and the amount

of time spent in the chamber. Hence, it is recommended to have a stop-watch ready beforehand and to set it immediately once the after pouring in the catalyst. Upon contact, the user should immediately start mixing the two materials together thoroughly, a process which should take no longer than 3 minutes to complete. The amount of time it takes for the majority of the trapped air to escape away varies depending on the material used as well as how much material is within the chamber. However, it was found that for $300mL$ of Vytaflex-20 resin material, it usually takes about $4-6$ minutes within the chamber before the liquid resin really starts to fizz up. And up to the 15 minutes before the majority of the air bubbles are removed from the resin. Make sure that the chamber is properly sealed beforehand, as any leaks will prevent the pressure in the chamber from getting low enough for the air bubbles to escape. The mixture should be removed from the chamber before the stop-watch reaches the 20-minute mark, regardless of how many air bubbles still remain. If the de-gassing process was successful, the resin must then be poured directly into the mold before it starts to harden.

3.3 Footpad Design Iterations

The sole-sensor went through multiple design iterations before finally settling on a working model. This section goes into great detail about the design decisions that went into each iteration of the sole-sensor in order to get a functional sensor working. While there were major differences between the versions, they all followed the same basic design scheme. In all versions, three FSR sensors are placed at select location along a 3D-printed "footpad" component. The locations of these sensors correspond to the main pressure map areas of the human foot - the "Heel" at the back of the foot, and the "Ball" towards the front. Two FSRs are placed at the "Ball" area, for

as can be seen in figure 3.5, the in-plantar pressure in Ball is distributed across the entire width of the foot, as opposed to being concentrated about a single point. As such, it makes sense to place two FSRs in this area as doing so allows the AFO to also track whether or not the Center-of-Pressure in leaning to the side of the foot. Only one FSR sensor is placed on the "Heel" location, as the pressure in this area remains concentrated along the mid-line of the foot.

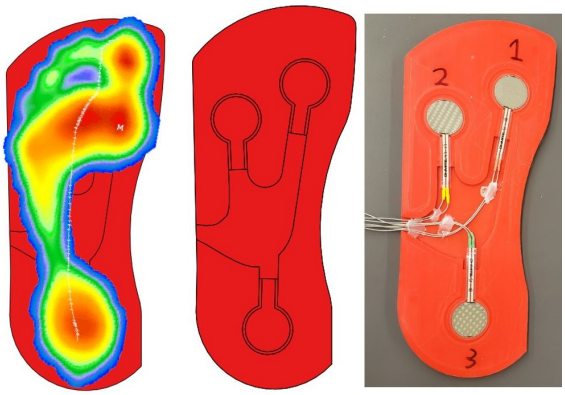

Figure 3.5: The FSRs placed on the "footpad" component, corresponding the the Foot-Pressure map taken from [20]

3.3.1 Design 1:

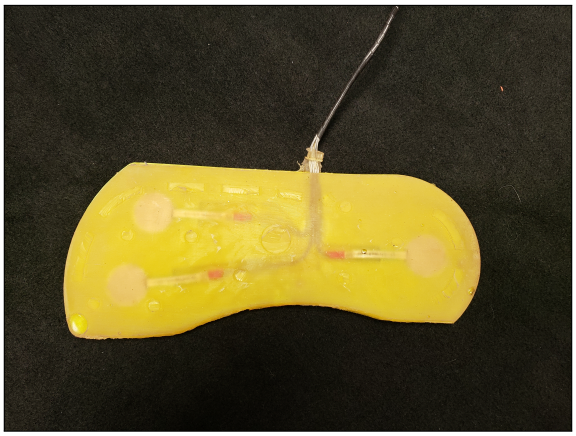

Figure 3.6: First Iteration of the Sole-Sensor. 3 FSR sensors encased within an even, 7mm-thick layer of Vytaflex-20 polyurethane rubber.

Description

The overall design for the first iteration of the force-sensing sole-sensor is fairly straightforward: Three FSR sensors are placed at select locations on a 3D-printed "footpad" component, corresponding to the actual force-concentration areas on a human foot. These sensors are then wired up, glued into place, and then covered in a 7mm thick coating of Vytaflex-20 polyurethane rubber. The resin material is distributed evenly throughout the mold, resulting in a thick, flat shape that covers the entire area of the footpad. A flat shape was chosen in order to maximize the amount of surface area that comes into contact with the ground, as that in turn would increase friction and better prevent the AFO from slipping while in use.

Resin Mold Design

The mold-shell used itself is split into top and bottom halves, both of which were 3D-printed. The Top-Half component is where the resin material gets poured into and contains the negative of the desired resin shape. The bottom half, meanwhile, has only a small cavity for holding the 3D-printed footpad component in place, as well as spots to securely mount the top half to it. Because these components are slightly larger than that of a human foot, their dimensions exceed the printing bed areas of most commercially-available 3D printers. As such, special care had to be taken in order to get these components manufactured. The bottom shell had to be split into two separate components in order to be printed in a safe and timely manner. The Top-Half component, however, could not be split into separate halves without compromising its main function of forming the shape of the resin. To get around this, the Top-Half had to be printed vertically, in a specialized printed with an extended printer-bed, in a print job that took over 19 hours to complete.

The design of the casting mold went through multiple minor iterations itself in

order to get the final shape right. The initial design had only a few tabs on the Top-Half component that loosely held it in place, lacked air holes, and had sides that lay completely flush with that of the bottom half. This resulted in a mold shell that allowed resin material to easily leak out. What material remained inside the shell could not even spread evenly throughout the mold, as the pockets of air trapped inside the shell occupied that volume. This resulted in the failed sole-sensors shown in figure 3.7, where the front and back of the sole-sensors are missing a significant portion of the resin.

Figure 3.7: An example of what can go wrong when trying to cure the rubber. In this case, air-holes were not provided in the mold-shells used during curing, prevent the air pockets trapped within the mold from being able to escape.

The next version of the mold shell was designed with the goal of keeping material from leaking out in mind. A series of 8 tabs were added to both the top and bottom components, with threaded holes for a 1/4" Diameter screw located in the center of each. This would allow both halves to be fastened together before pouring in the resin, forming a tight seal less than $0.5mm$ thick to limit leakage. Additionally, thin walls were added to the sides of the bottom shell, creating an additional boundary should any material make it through the seal. Air slots with a thickness of $6mm$ were placed along the outer edges of the sole, to allow the air trapped there to escape. These changes proved to be successful, with the resin forming into the desired shape without any major air pockets getting in the way. The components for this mold

shell are shown in 3.8, with the resulting sole-sensor placed in-between them.

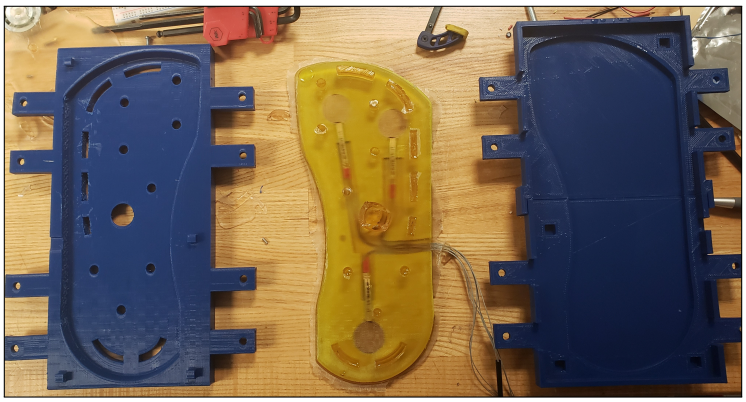

Figure 3.8: 1st Iteration Mold-Shell: Both halves of the shell are visible, with a freshly-released Sole-Sensor between them.

Results

When the resin finally finished curing, the initial results of the component looked promising. Individual testing of each FSR showed that, despite being encased within a thick layer of polyurethane rubber, they could still react to forces applied to the rubber directly on top of them. However, it quickly became clear that there was a major problem with the design. During routine testing of the device, it was found that when the user placed their foot directly on-top of the sole-sensor, as they would do if they were to operate L.A.R.R.E, all 3 FSRs would return analog readings of 0 no matter how hard the foot was pressed. Much work went into identifying the cause the the malfunction. Several tests were run on the 1st iteration, to try an identify the cause of the problem. The circuit design was re-inspected to see if any FSRs were shorting out somewhere, but that quickly became clear that was not the case. One test showed that it was possible to still activate all 3 FSRs using the users foot if wooden platforms were placed directly underneath the FSRs before stepping down. Several more tests re-confirmed this to be the case. This meant

that the problem with the Sole-Sensor was not anything electronic, but with how the resin-covering was shaped.

Figure 3.9: The 1st version of the Sole-Sensor did return values when forces were applied directly on the resin areas directly above the FSRs, as shown on the Left. However, stepping on the footpads directly with one's foot (Right) causes the pressure to be distributed throughout the resin medium, reducing total displacement such that no material gets pushed up against the FSRs. This results in the FSRs returning values of 0, i.e. "no load", even when a person is standing on top of the device with one leg.

The layer of polyurethane rubber that encases the FSRs and footpad is distributed evenly throughout the mold, creating a thick, flat surface once the resin finally cures. This was by design, as the flat surface helps to maximize the total area that comes in contact with the ground. On this aspect, the design succeeded, as during testing the AFO never once felt as though it could accidentally slide across the floor. However, this shape also results in the pressure being applied across the entire area of the footpad, rather than being concentrated around specific locations. This causes the amount of force applied at a specific point on the sole to be minimized, which in turn reduces the total amount of displacement that occurs within the resin. The result is that not enough resin is displaced in order to apply pressure to and activate individual FSRs, hence why they constantly returned digital values of 0 even when a person was standing on the Sole-Sensor. However, more direct applications of force, such as poking the resin with one's finger directly above

the locations of the FSRs, will displace the material enough to activate the FSRs. Hence, the reason why we initially believed the Sole-Sensor was working as intended.

3.3.2 Design 2:

Description

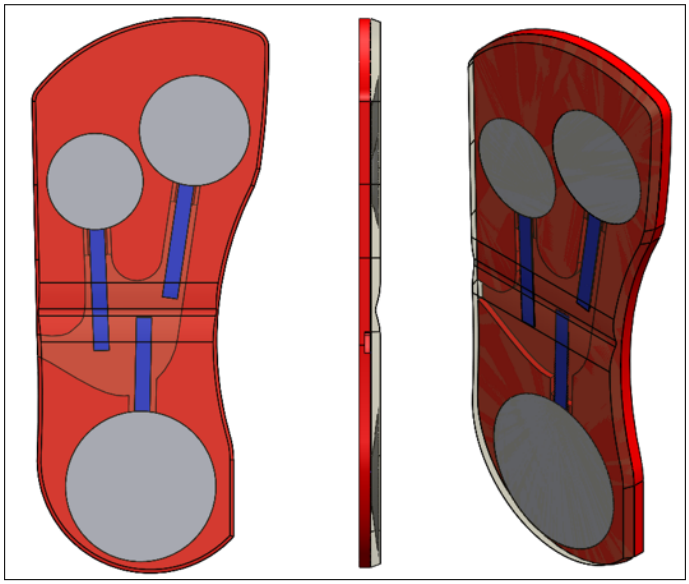

Figure 3.10: Main design of the 2nd Iteration Sole-Sensor. A channel carved in the resin separates the Ball and Heel sections, while three "Force-Cups" lie embedded within the resin, only 1mm away from the surface.

Even with the problem identified, there was still a number of issues left uncertain. While it was clear from the testing that there should be a gap in the resin between the Ball and Hell areas in order to activate the FSRs, what was not clear at the time was how large that gap should be. Furthermore, removing material from the sole could have its own set of issues, as less material in contact with the ground means less static friction to hold the AFO in place. Even with the gap, there would still be no guarantee that the Ball FSRs would still activate. While in theory it would be possible to get the 1st iteration working by simply carving out excess resin material,

the resulting sole-sensor shape wouldn't be replicable using the existing molds.

Hence, the 2nd iteration mainly served as a test bed for potential ideas to get the Sole-Sensor working. To keep things relatively consistent, the main change within the shape of the sole would be the addition of a channel separating the ball and heel areas. The width of this channel was determined through testing with the prior iteration, wherein wooden platforms would be placed directly underneath the Ball and Heel sections of the sole-sensor before the user stepped on it. This has the effect of activating the FSRs when pressure is applied, albeit not always reliably. The distance separating these platforms would be incrementally reduced, until stepping down would no longer activate the FSRs. From these tests, it was determined that the minimum seperation distance needed to still activate the FSRs between the Ball and Heel areas would be approximately $85.7mm$. There were other slight changes were made to the design, such as reducing the overall thickness of the resin layer from $7mm$ thick to $5mm$. The placement of the FSRs on the footpad also received a slight adjustment, with the Ball FSRs being moved slightly closer to the center. This was done such that the FSRs would more accurately line up with the actual pressure areas of the human foot.

Furthermore, at the recommendation of my advisor, this iteration would introduce a potential new component into the sole-sensor design. The thinking was, because the resin shape distributes all forces acting on it such that the effect they have on the FSRs is essentially negligible, there should be a component within the resin that helps redirect said forces directly to the FSRs. These items should have only a very thin amount of resin placed above them, with a wide surface area on the top that tapers down into a much smaller area towards the FSRs, in order to help maximize the effects of the displacement through the component. Additionally, they should also be made out of a flexible material, such as Ninja-Flex or other kinds of

TPU, such that the components will be able to actually apply a force directly on the FSRs themselves. Hence, the addition of the 3.575mm thick Force-Redirection Cups, or Force-Cups. The inclusion of the Force-Cups, as well as the inclusion of the channel, are displayed in the CAD model shown in Figure 3.10.

Resin Mold Design

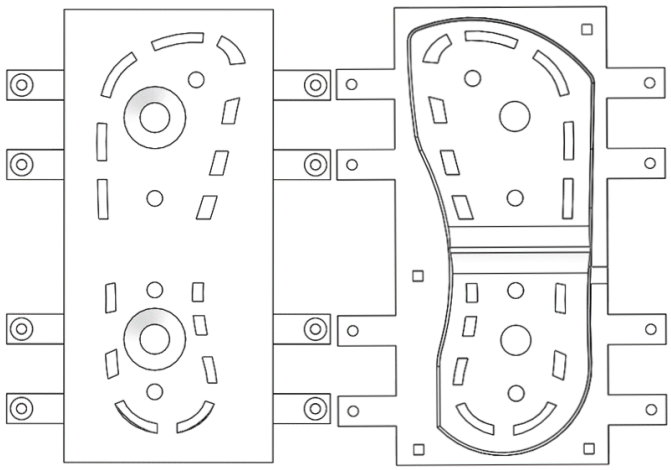

Figure 3.11: Mold-Shell design used for the 2nd iteration of the Sole-Sensor. Only the geometry of the top half needed to be changed. Extended "Groove" geometry within the mold-volume creates the channel that splits the 'Heel' and 'Ball' areas of the resin. To ensure even distribution of resin during the curing process, each section was given its own mold-pouring hole.

All the major design changes within this iteration were with the design of the resin-shape, while the 3D-printed footpad component remained unchanged. This allowed us to re-use the bottom-half of the Mold Shell from the 1st iteration. For the Top-Half component, the main change to the resin shape was the addition of the channel section. This was a fairly simple enough addition to put in, as all it required was taking a direct negative of the new resin-shape CAD through SolidWorks. In order to minimize any chance of the mold shell getting stuck to the geometry, the channel itself was designed with a semi-circular cross-section, as can be seen in Figure

3.10. This channel-negative leaves the gap between the footpad and the Top-shell to be only 2.5mm tall. Because the mold will have trouble moving through such a tight gap, it was decided to have two separate mold-pouring holes for both the Ball and the Heel sections. The air-slots were kept at the same positions as the prior iteration, though some of the smaller air-holes did have to be moved so as to not interfere with the channel. Like the prior iteration, 8 tabs with screw holes were attached to the sides in order to help fasten the mold down.

Results

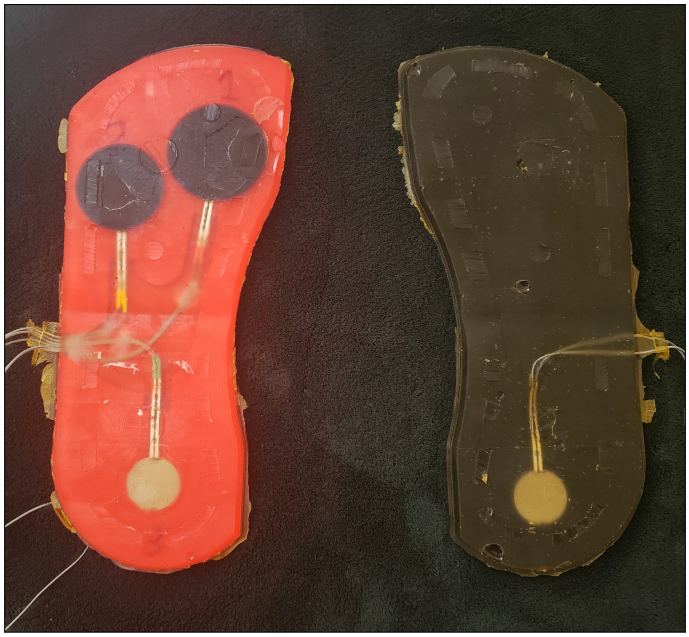

Figure 3.12: Finished versions of the 2nd iteration Sole Sensor. (Right) First set with only 1 FSR, used to test the effect of the channel on FSR readings. (Left) Second set with all 3 FSRs and Force-Redirection cups, made to test the effectiveness of the cups on FSR readings.

Two sets of sole-sensors were made using this design. The first set was made in order to test whether or not adding a channel into the resin was effective at activating the FSRs. For this reason, no Force-Cup components were included in

this version. Only a single FSR was used in order to conserve resources, placed at the heel as that location would be the most effected by the addition of the channel. The resulting component can be seen in Fig 3.12 on the right. Tests with this particular component proved relatively successful. No matter how a person stood on the footpad, the Heel FSR still returned non-zero values as long as the pressure was applied.

The 2nd set was made with implementing the force-cups in mind. Three different types of Force-cup components were printed, however only the two for the Ball FSRs were used for this set. This is because the results from the previous set showed that the Heel FSR could activate using the channel alone, and the force cups were more useful for the Ball FSRs anyways. That, and for the fact that including it would completely block any resin poured in from the Heel-section pour-hole from reaching the footplate component. So rather than remake a whole new Top-Mold Shell component, it was decided to simply leave the Heel Force-cup out of the design. This component is featured on the left side of Figure 3.12.

It became clear once the sole-sensor was pried out of the mold that the $1.425mmm$ gap between the top of the force-cups and the Top-Shell was not large enough to let the resin material flow through all the way. As can be seen in Figure 3.12, the resin was only able to cover the outer edges of the force-cups, while the center of both cups remains uncovered. This development makes it difficult to get readings from the Ball FSRs when stepping down, as there is not enough resin being compressed to in turn compress the Force-Cups. To further complicate matters, it was also found that even the Heel FSR, which seemed to respond well during the 1st set, was also having trouble activating in a reliable manner. This indicated that even implementing the resin channel into the design would not be enough to get accurate readings out of the sole-sensor.

3.3.3 Design 3:

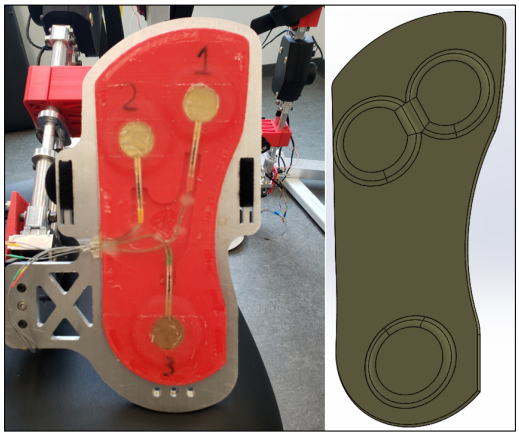

Figure 3.13: Final version of Sole-Sensor installed within the AFO footplate. The three small "bubbles" located directly above the FSRs help to redirect all displacement in the resin to the FSR areas

Description

For the 3rd version, it was known going in that trying to preserve the resin material was not going to work. Hence, the focus of the new design would be to rework the mold-shape so that the only areas that come into contact with the ground are those directly above the FSRs. This would allow any pressure acted on the resin to be transferred directly onto the areas directly above the FSRs. Doing this would also eliminate the need for the force-cups, hence why these particular components were removed from the design. Before, the concern over removing material was whether or nor that would make the AFO more susceptible to sliding on a smooth surface. However, given that none of the prior iterations experienced any amount of sliding during testing, this concern was fairly non-substantial at this stage. That being said, the circumference of these resin "islands" is offset from the diameter of the FSRs by about $15mm$. This was less about maintaining static friction and more so that the user would not have to stand on small rubber pegs whilst operating

the exoskeleton. The 'resin islands' maintained the $5mm$ thickness from the prior iteration, however the non-island portions only had around $2.5mm$ of resin covering the footpad.

Resin Mold Design

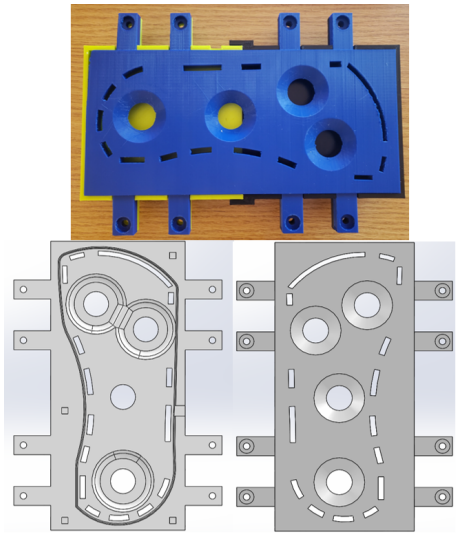

Figure 3.14: Top-Half Mold-Shell component used within the 3rd iteration of the Sole-Sensor. (Top) The actual Top-Half component, attached to the Bottom-Half component ready to start molding. (Bottom) SolidWorks CAD model of the Top-Half component, with both the top and bottom geometries visible.

Like the 2nd iteration, the design of the footpad component remained unchanged. Hence, the Bottom-Half Mold shell component from the 1st iteration could once again be reused for this design. For the Top-Half Shell, 4 Mold-Pouring holes were included in this design: 3 for "resin islands", and 1 for the middle section of the footpad. The shell was designed not to accidentally impede the flow of resin, hence the reason why the non-island sections had a thickness of $2.5mm$ rather than $1mm$. Like all prior versions, the Top-Shell component has 8 tabs with 1/4"-screw threads for fastening it to the Bottom-Shell. The geometry of the mold was made using the same technique as the 2nd iteration, wherein a negative of the desired resin geometry

would be taken using Solidworks then formed into a new part. One slight change compared to previous versions is that the thickness of the Top-Shell component was slightly reduced by about $2mm$. This was done in order to reduce the overall printing time from 21 hours to 19 hours. The full design is shown in full within Figure 3.14.

Results

This design proved to be a success. Preliminary tests showed that the FSRs finally activated when the user stepped down on the footpad, as opposed to just returning values of 0. Additionally, even though the amount of resin area that comes into contact with the ground had been significantly reduced, there was still enough resin in contact with the ground to prevent the AFO from sliding. The success of this design allowed us to move forward with proper CoP testing, the results of which are described in length in Chapter 4.

Chapter 4

Analysis and Testing

4.1 Static FEA Analyses

In order to ensure that the joint would not buckle, the CAD models were run through several static FEA stress analyses before they were manufactured. The components that went through this process are: 1) The Joint Axle; 2) The Ball-Bearing plates; 3) The "Shank Arm with Collet" component; 4) The footplate. All FEA simulations were run using the built-in SolidWorks SIMULATION settings. With the exceptions of the Axle Shaft, the majority of components simulated here were manufactured using 6061 $T6$ Aluminum alloy. The Axle Shaft, meanwhile, was manufactured using 304 Cold-Finish Stainless Steel. The material-properties tables for all these materials can be found within the Appendix section of the paper.

4.1.1 End-Cap Coupler FEA

External Load Placements

The expected load of $3580N$, as defined earlier in Chapter 1, is applied to the top thin extension of the component. This is the area of the component that comes

into contact with the "End Cap", and hence is also where all the load from the exoskeleton is applied to.

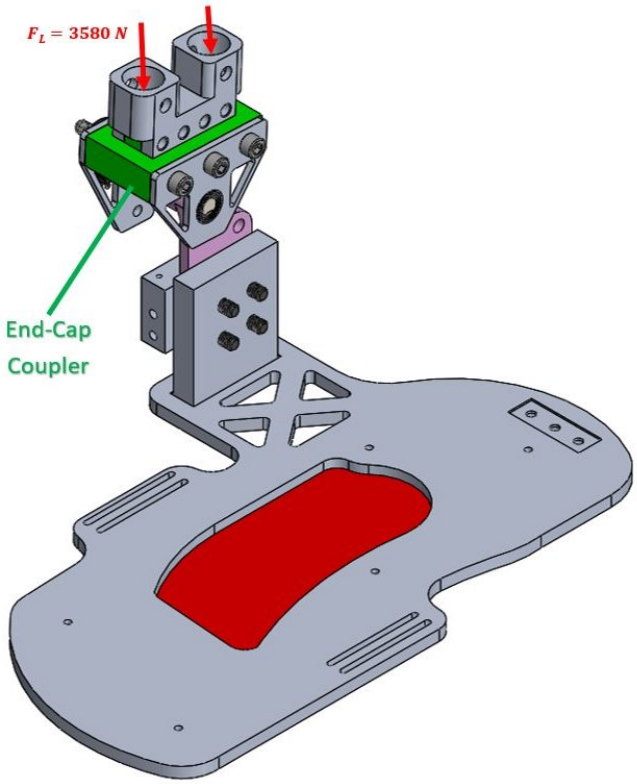

Figure 4.1: Position of the End-Cap Coupler component within the greater AFO assembly (colored green) as the static load from the rest of the Exoskeleton is applied.

Fixtures

In order to simulate the component's placement within the greater AFO assembly, all seven mounting holes in the component were treated as fixed geometries within the simulation. This acts in place of the $1/4" - 20$ Threaded bolts used to connect the component to the rest of the system.

Results

The results from this particular Static simulation show that the Von Mises stresses the End-Cap Coupler experiences do not exceed its yield strength. Additionally, the majority of the stress concentrations occur at the topmost tab, where the load is applied, and not on any other portions of the geometry. This is ideal, as any stress concentrations along the edges could result in fracturing.

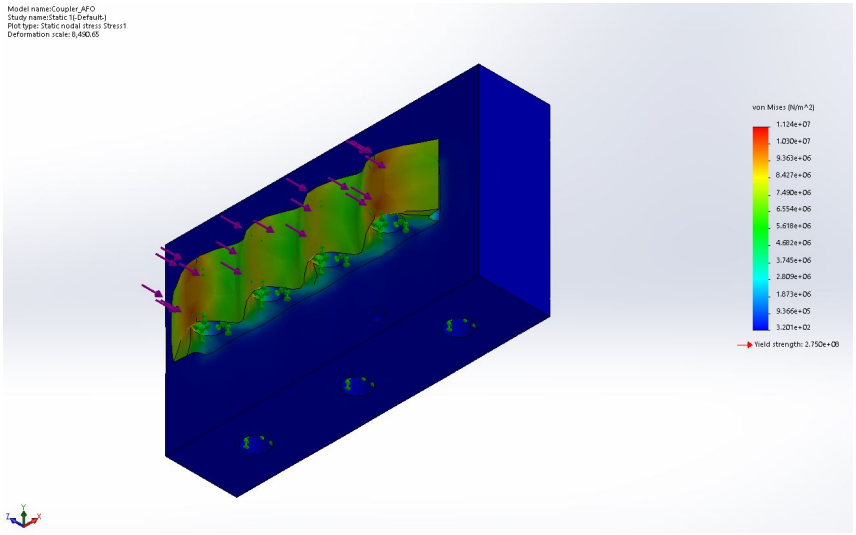

Figure 4.2: FEA Simulation Results of Load from L.A.R.R.E being applied to the End-Cap Coupler component.

4.1.2 Ankle-Joint Axle Shaft FEA

External Load Placements

For the join-axle component, the majority of the forces acting on the object would be on the ends of the shaft, where the ball-bearings would attach to. These sections should be strong enough to hold up desired maximum static load of $3580N$ from the Exoskeleton.

In addition to the forces applied on the axle ends, the Joint-Axle component

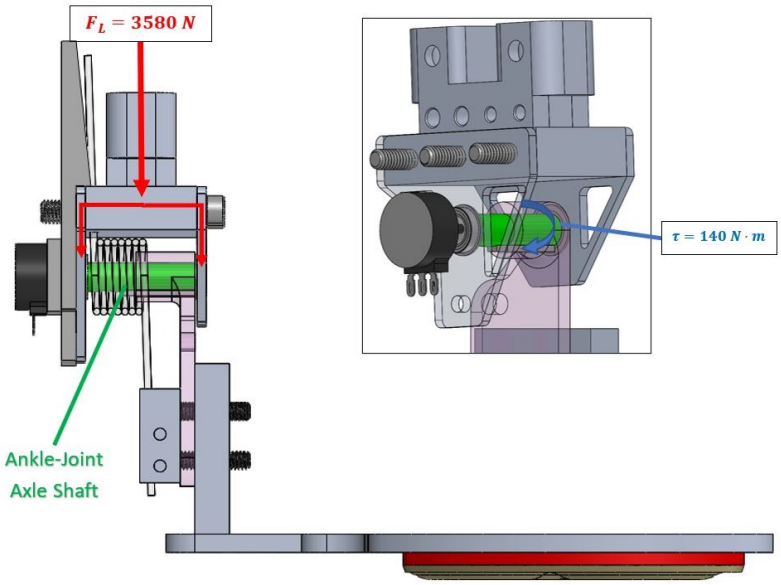

Figure 4.3: Figure indicating the expected Static Force and Dynamic Torque loads placed on the Axle Shaft component (colored green) when within the AFO system.

is also designed to undergo a twisting motion when dorsiflexion occurs. It was originally designed to connect with the "Shank Arm with Collet" component through the addition of a square-profile shaft key, in order to ensure proper force distribution down to the footplate. When the user engage in either dorsiflexion or plantar-flexion, this motion causes the "Shank Arm with Collet" to twist about the joint axle, and apply pressure on the key-shaft. The key-shaft in turn applies a torque on the outer-walls of the joint-axle, causing it to twist as well. As such, the axle must also be able to withstand this torque from the key-shaft in order to properly function as a joint. For the FEA, the torque was set to $140Nm$.

Fixtures

The circumferences of both axle shaft-ends are defined as Bearing Fixtures within the assembly. This helps to simulate the interaction between the axle shafts and the bearings that would normally surround them within the assembly. On the part

of the geometry where the diameter of the end-shafts change to the diameter of the main shaft, the faces of said geometry were set as fixed ends.

Results

The results of this Static-load simulation show than, when under the expected loads, the Von Mises stresses on the Joint Axle never exceed the yield strength of the material, which, according to the simulation, is at $6.2 \times 10^8 Pa$. As shown below in figure 4.4, no major stress concentrations appear on the device, even around the sharp edges around the keyshaft-channel.

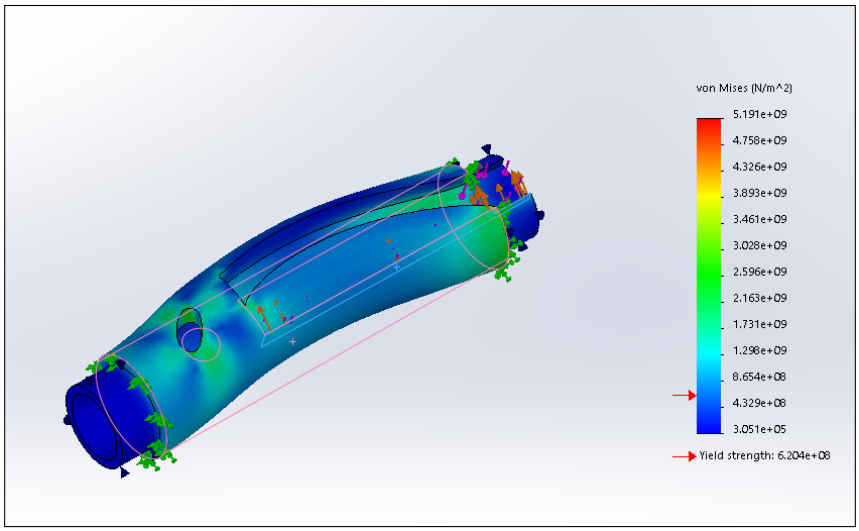

Figure 4.4: FEA of Ankle-Joint undergoing forces on the bearing ends and torque applied on the key-shaft wall. Picture shows stress concentrations on component.

4.1.3 Ball-Bearing Mounting Plates FEA

External Load Placements

For both versions of the Bearing Mounting Plates, two sets of external loads are applied on the components. The first is a load of $3,580N$ placed around the inner-edges of the bearing-housing hole. This represents the expected force placed on

the plate as the load from the exoskeleton causes it to press itself against the ball-bearing. The second is another load of $3,580N$, but placed around a thin area just directly around the bearing-hole. This represents the outer-lip of the ball-bearing component as it press-fits itself into the plate.

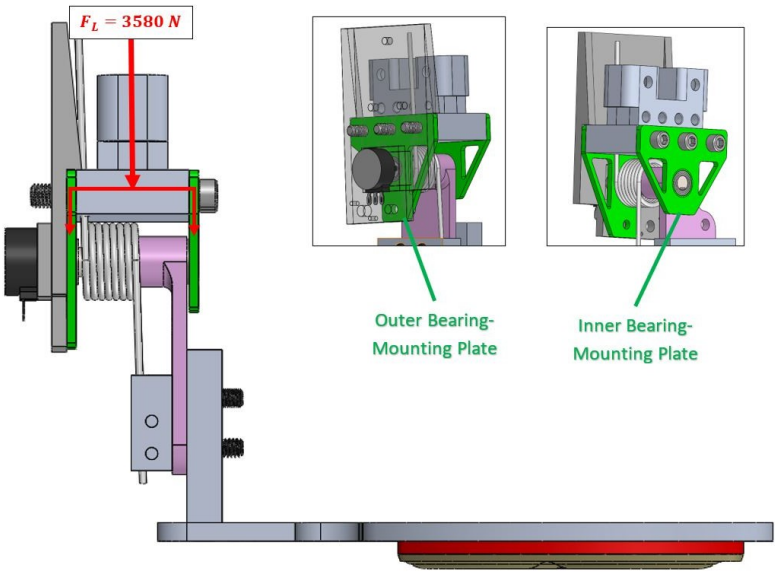

Figure 4.5: Positions of both Bearing Mounting Plates (colored green) within the greater AFO assembly as load from the Exoskeleton it split between the two components.

Fixtures

As both versions of the Bearing Mounting Plates would be fixed to the rest of the assembly through the $1/4" - 20$ threaded screw holes, for both versions all three screw mounting holes are set as static fixtures within the FEA simulation. An additional Bearing-Mount fixture is also placed on the edges of the larger hole located in the component's center, in order to simulate the placement of the Ball-Bearing.

Results

The results of the FEA simulation, displayed within figure 4.6, show that both versions of the Bearing Mount plates are able to withstand the maximum amount of expected load placed on them without buckling or fracturing.

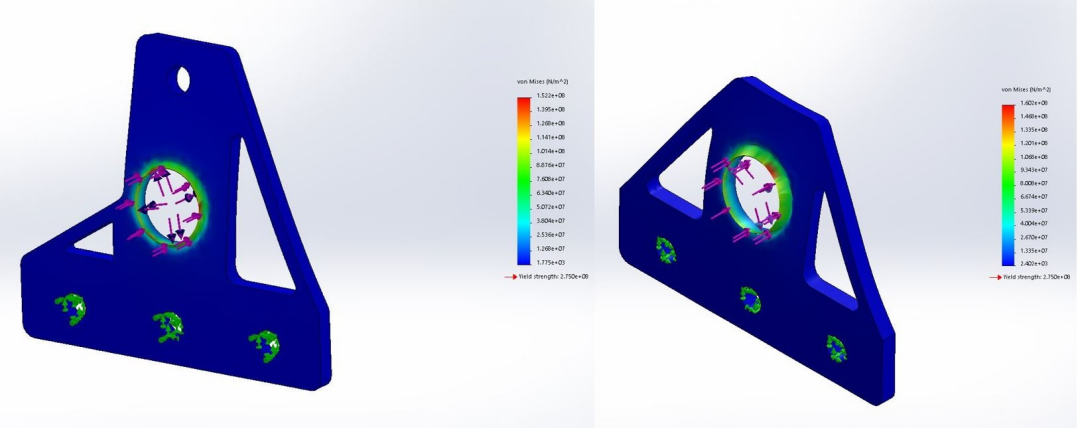

Figure 4.6: Static FEA analysis display of Von Mises Stresses of both versions of the "Bearing Mount Plate".

4.1.4 Shank-Arm FEA Test

External Load Placements

For this component, the expected external load from the exoskeleton, $F_L = 3580N$, is assumed to be applied through the key-slot channel. This is because the Shank-Arm was originally designed to interface with the Ankle-Joint Axle Shaft through the key-shaft that would've gone into this channel. Hence, the load was set to this surface within the simulation.

Fixtures

The four mounting holes, where the $1/4" - 20$ Threaded screws would mount the Shank Arm to the Footpad sub-assembly, are set as fixed geometries. Additionally,

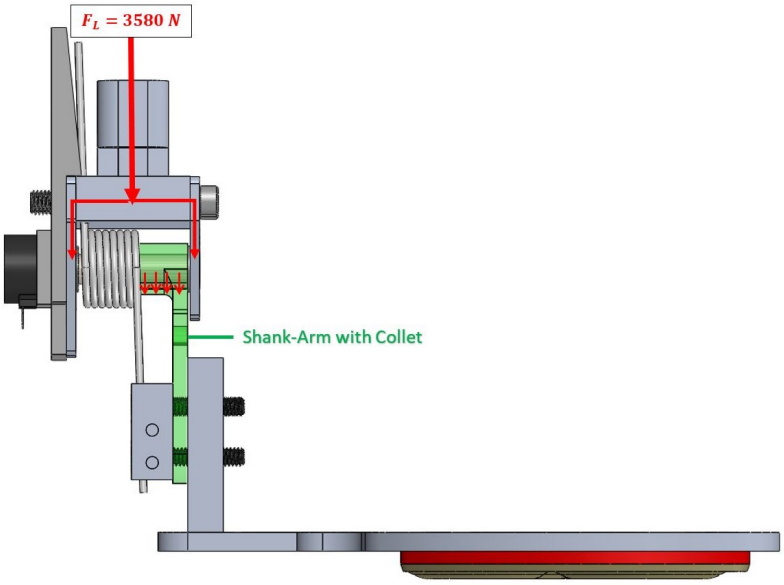

Figure 4.7: Position of the Shank-Arm component (colored green) within the greater AFO assembly as the static load from the Exoskeleton is applied.

as the Shank-Arm is designed to be pinned between the Spring-Block and "Outer Ankle Connection Plate" components, the back-face of the component is also set as a fixed geometry.

Results

As displayed within Figure 4.8, the majority of stresses placed on the component concentrate themselves directly below the area of the collet where the static load from the Exoskeleton is applied. Fortunately, the Von Mises stresses do not exceed the yield strength of the component, which according to the simulation, is at $2.75 \times 10^8 Pa$.

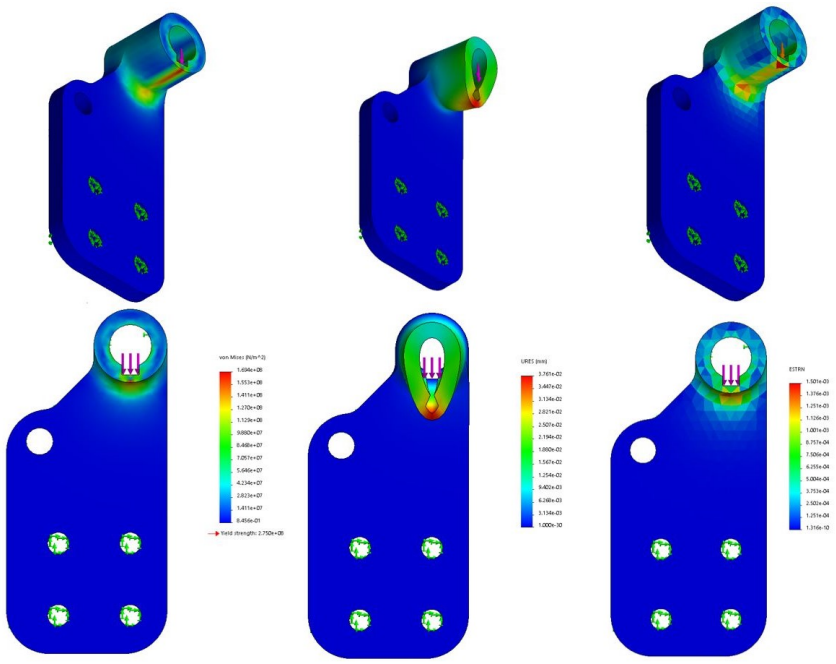

Figure 4.8: Static FEA analysis of the "Shank-Arm with Collet" component. Test was done by making the mounting holes fixed and applying a force of $3580N$ directly onto the Key-slot. The Von Mises Stresses, Displacement, and Strain on the component are displayed in full.

4.1.5 Footplate Component FEA

External Load Placements

For this simulation, two separate Force loads were placed onto this component. On the slot where the Ankle-Mounting Plate installs, the weight load of the L.A.R.R.E exoskeleton, $F_L = 3,580N$, is applied. Another, smaller load is applied on a small area towards the front of the component, which helps to simulate the pressure applied by the wearer's foot as they stand on the component. This area corresponds the to ball of the human foot, where the majority of pressure is concentrated. Assuming that the wearer has the average mass of an adult human male, which for this paper is defined at $73kg$ [15], then the amount of force their foot would apply to the footplate would be around $F_{F_{Pressure}} = 716.13N$.

Fixtures

In this simulation, the only fixed geometry is the thin cavity on the bottom of the footplate, where the Sole-Sensor would normally be installed. This is because it is this area where all the normal reactive force from the ground will be applied to when the user stands on the AFO.

Results

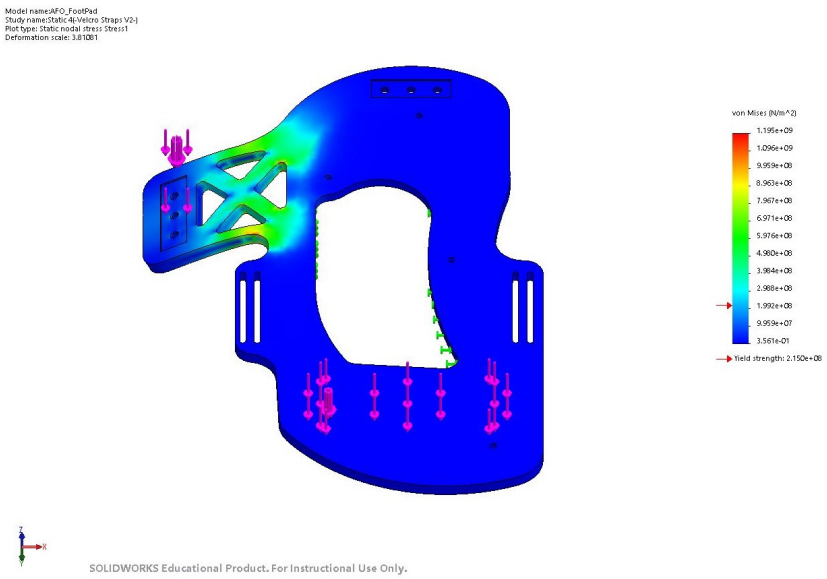

Figure 4.9: Static FEA Analysis of the Footplate component, with loads of $3,580N$ and $716N$ applied on both the "Ankle Mounting Plate" slot and the Ball areas, respectively.

The FEA study combining the two external loads together shows that the amount of force applied by the user's foot has a negligible effect on the component when compared to the load from the exoskeleton. As can be seen in figure 4.9, most of the stresses concentrate around the area of the tab that surrounds the mounting-plate slot.

4.1.6 Assembly FEA Simulation

Due to the limitations of the Solidworks FEA Simulation software, a static load simulation on the "Outer Ankle Connection Plate" by itself cannot be performed without also modifying the components geometry to properly simulate the effects of the loads. As the component works to connect the "Shank-Arm with Collet" and "Footplate" components together, it makes more sense to run a simulation using an Assembly of just these three components to see how the load is transferred through the "Outer Ankle Connection Plate".

Parts Used

The components used for this test were the "Shank Arm with Collet", "Outer Ankle Connection Plate" and the "Footplate". The purpose of this test is to see how the load acting on the Shank Arm gets transferred through to the Footplate.

External Loads

The only load used within this simulation is the estimated $3,580N$ weight from the L.A.R.R.E used throughout all the other tests. This load is applied at the bottom of the keyshaft channel geometry of the "Shank Arm with Collet" component.

Fixtures

The only fixture placed in this simulation is the bottom cavity of the Footplate, where the Sole-Sensor would normally install into. The back of the Shank Arm component is already coincidentally mated to the surface of the Outer-Ankle Mount connection plate, but neither surface is treated as fixed geometry. The $1/4" - 20$ threaded mounting holes were originally treated as fixed geometries, however

doing this caused the simulation to concentrate all the forces on the Shank Arm component, as opposed to spreading them out throughout the assembly.

Results

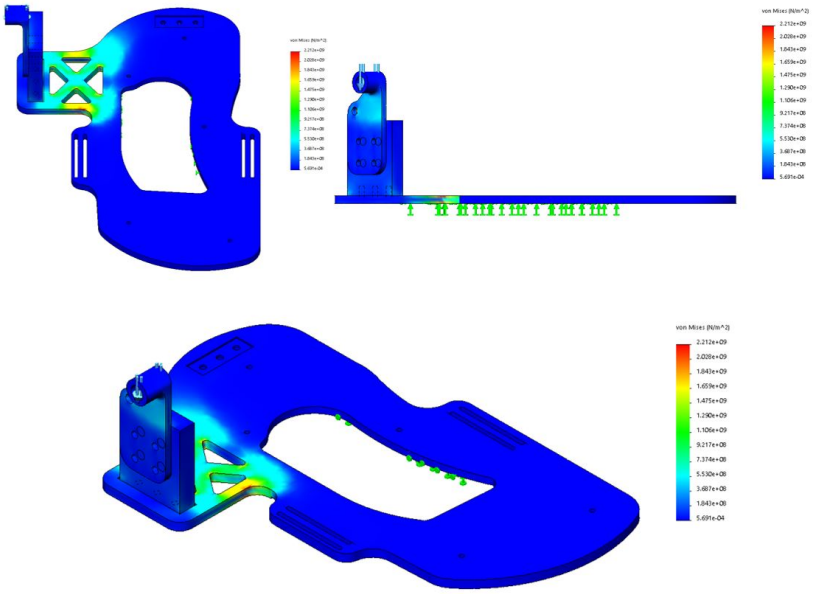

Figure 4.10: Static Load Deformation results showing how the load placed on the "Shank Arm" gets transferred through the "Ankle Joint Connection Plate" component and into the "Footplate. The majority of the Von Mises Stresses occur mainly on the Footplate component, with some stresses concentrating on the Shank-Arm directly beneath the collet.

As can be seen within figure 4.10, the majority of stresses are transferred through the "Outer-Ankle Connection Plate" and into the Footplate. These stresses concentrate themselves around the area where the Connection plate attaches to. This lines up with the results of the FEA Simulation focusing solely on the Footplate component, shown in 4.9.

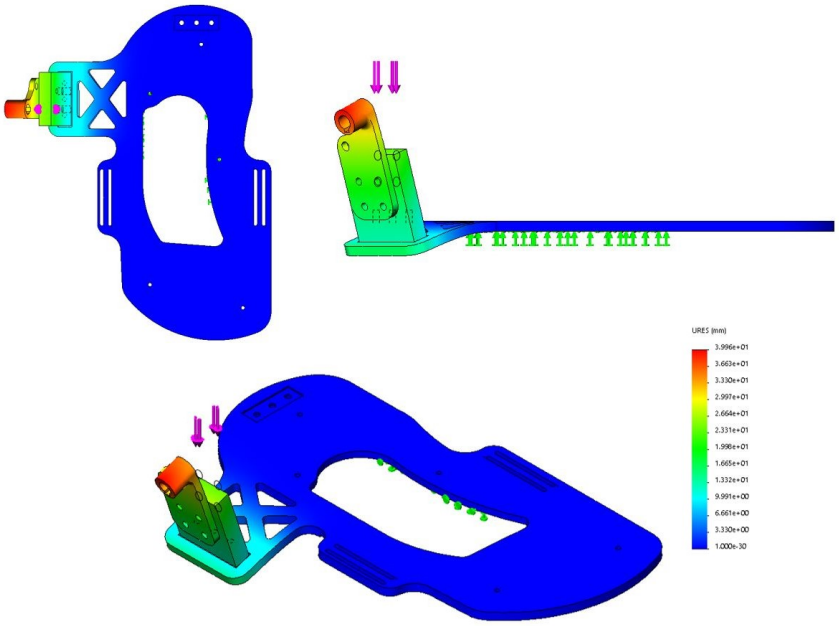

Figure 4.11: Displacement results from the FEA Simulation.

4.2 Single Foot MOCAP Test - Footsole Sensor Readings

4.2.1 Test Description

The successful development of a working Sole-Sensor allowed us to move forward with proper testing of the AFO. The first major test was a motion capture study held within WPI AIM Laboratory's Vicon Room. The study was designed to compare the Center-of-Pressure (CoP) readings from the AFO Sole-Sensor with that of Force-Plate installed within the lab. Additionally, the test would also compare the performance of the $3rd$ iteration Sole-Sensor to that of the $1st$ iteration Sole-Sensor, to illustrate the difference that the different design has on the readings. While it was already known that the 3rd version would return values once pressure was applied, this would be the first time the Sole-Sensor would be used in an actual scientific

test.

Test Set-Up

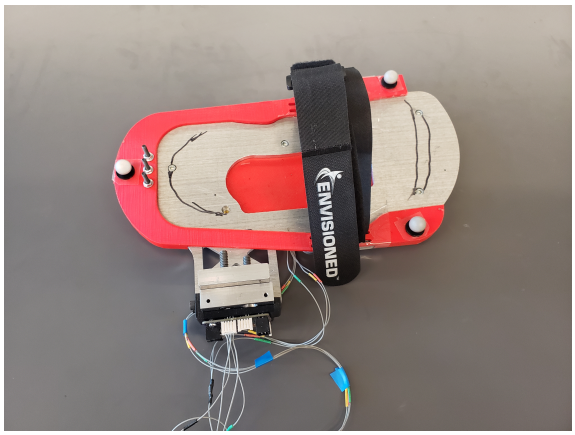

Figure 4.12: AFO with Mocap Horseshoe bracked and Vicon markers, right after testing.

In this study, a single AFO unit, detached from the greater L.A.R.R.E system and with working sole-sensor installed, is placed in the middle of the MOCAP Camera area on top of one of the Force-Plate units. For this study, only the Right-Leg AFO was used. Attached to the AFO is a specially made "Mocap Horseshoe" component, which wraps around the AFO and holds 3 MOCAP markers in place close to the FSRs, as shown in figure 4.12. After calibrating both the Vicon Cameras and Force plates, the human operator enters the testing area and straps their foot into the AFO. For this study, a trigger signal will be sent from the Vicon set-up to the on-board Arduino to tell it that the trial has started and to start collecting FSR data. During each trial, the human operator keep the AFO at a specific position for 15 seconds, before moving it into another position for an additional 15 seconds. Depending on the position of the AFO, different FSRs on the Sole-Sensor will be activated or deactivated. The Arduino prints out readings taken from the FSRs within the serial monitor, and when the trial is done, exports that data as a

.CSV file. The order of these positions are: Flat-Foot → Toe-Down → Flat-Foot → Heel-Down → Flat-Foot. Given 15 seconds per foot position, and 5 positions in total, each trial would last for an average length of 75 seconds.

4.2.2 Results and Analysis - Sole-Sensor Version Differences

The results from these trials show a clear difference between the 1st and 3rd iteration Sole-Sensors in terms of how they're able to react to foot pressure. As the baud rate for the Arduino was set at 9600 for the trials, data points would be recorded at a rate of roughly 1-data/second. As such, it was relatively straightforward to correlate changes in the recorded FSR values alongside when the user changed their foot position. In order to simplify the data, all FSR values were "binarized", such that all returned values of < 200 were treated as noise, while any values > 200 were considered to be indicative of the FSR being activated via pressure.

1st Iteration Sole-Sensor Results

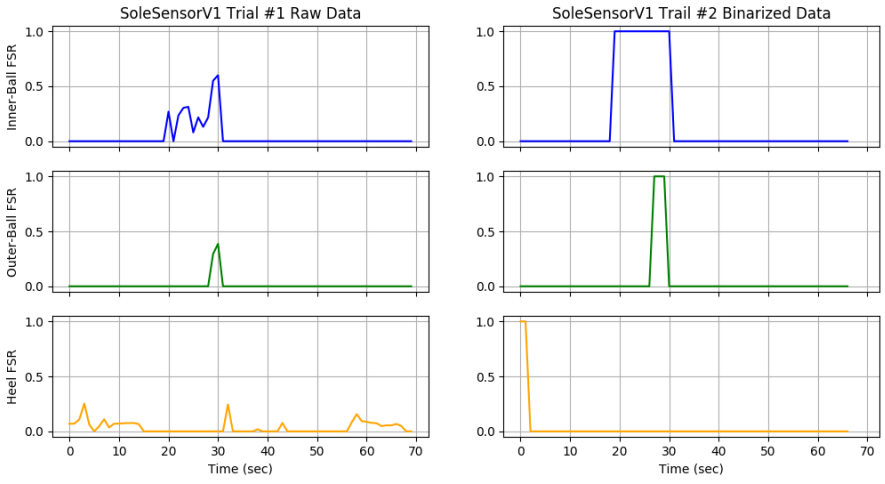

Figure 4.13: Sole-Sensor Version 1 - Trial 1 Raw vs. Binarized FSR Sensor Data Results

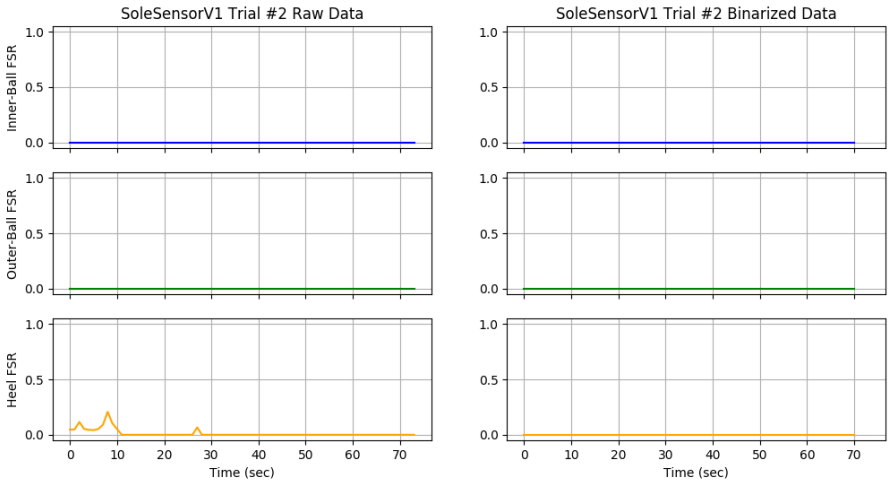

Figure 4.14: Sole-Sensor Version 1 - Trial 2 Raw vs. Binarized FSR Sensor Data Results

The binarized results of the two trials with the original Sole-Sensor design, seen in figures 4.13 and 4.14, clearly show that this version of the device does not perform as desired. Since the same foot-position order of Flat-Foot → Toe-Down → Flat-Foot → Heel-Down → Flat-Foot every 15 seconds was followed, in theory the normalized results should show different FSRs activating depending on the position of the foot. Instead, in only one of the two trials did a single FSR actually activate at all(Fig. 4.13). These results show that having a completely flat sole-surface that evenly covers all three Force-Sensors is anathema to detecting the concentration of Forces placed on the AFO.

3rd Iteration Sole-Sensor Results

Binarizing the raw data returned from the 3rd Version of the Sole-Sensor shows a marked improvement in both the performance and consistency of the FSRs. As shown in Figures 4.15 and 4.16, FSRs were able to activate and deactivate consistently during the same time-steps of each trial. So much so that, converting the raw sensor data from each trial into either "On" or "Off" states results in the same

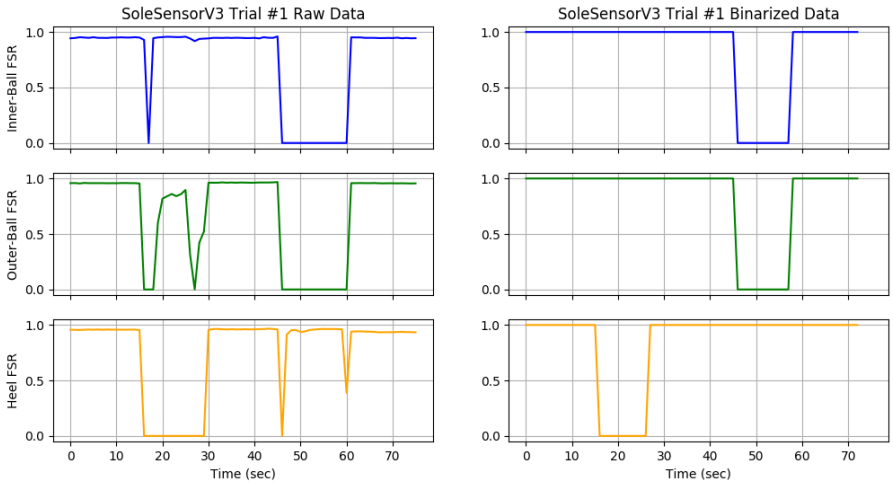

Figure 4.15: Sole-Sensor Version 3 - Trial 1 Raw vs. Binarized FSR Sensor Data Results

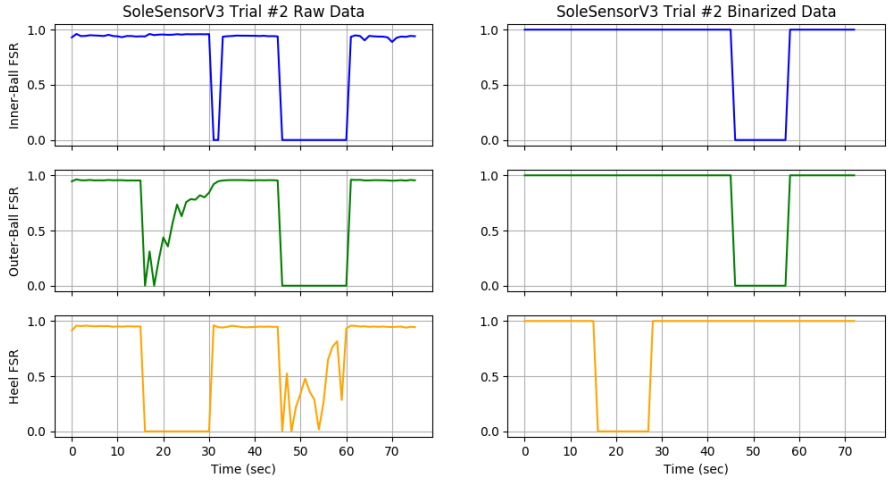

Figure 4.16: Sole-Sensor Version 3 - Trial 2 Raw vs. Binarized FSR Sensor Data Results

"Binarized" plot. This means that, using the 3rd Version, its possible to reliably detect foot position using the values returned by the FSRs.

Foot Position State-Table

Using the data collected from the MOCAP study trials, we are able to determine which FSR readings correspond to what Foot position. By looking at which FSRs

are activated (i.e. have readings > 0) at any point in time, its possible to determine what position the AFO is in at that moment. For example, the trial shows that when the foot is lying flat on the ground, enough pressure is being applied to all three FSRs in order to activate all of them together. Developing this further, we can create a State table for each Foot Position, wherein the FSR activation-states take the role as input bits.

FSR1 - Inner Ball	FSR2 - Outer Ball	FSR3 - Heel	Position-State
0	0	0	Foot not on ground
0	0	1	Heel-Down
0	1	0	Transition or Error
0	1	1	Leaning Outward
1	0	0	Transition or Error
1	0	1	Leaning Inward
1	1	0	Toe-Down
1	1	1	Flat-Foot

Table 4.1: Right-Foot AFO Position State-Table with FSRs as bits

4.2.3 Results and Analysis - Center-of-Pressure Vicon Marker Tracking

By comparing the magnitude of the values returned by the FSRs with their known positions within the AFO's local reference frame, defined within Figure 4.17 in units of mm, it becomes possible to both calculate and track the Center-of-Pressure position within the AFO. The Center-of-Pressure point shows where the majority of forces on the AFO are concentrated at any instance. In theory, when the user is in the flat foot position, the CoP should lie in the center-point between the Ball and Heel FSRs along the local Y-axis. Additionally, when the user is in the "Heel-Down" position, the CoP is expected to lie directly in the center of the Heel FSR, which is located close the the origin along the Y-axis. And when the user is in

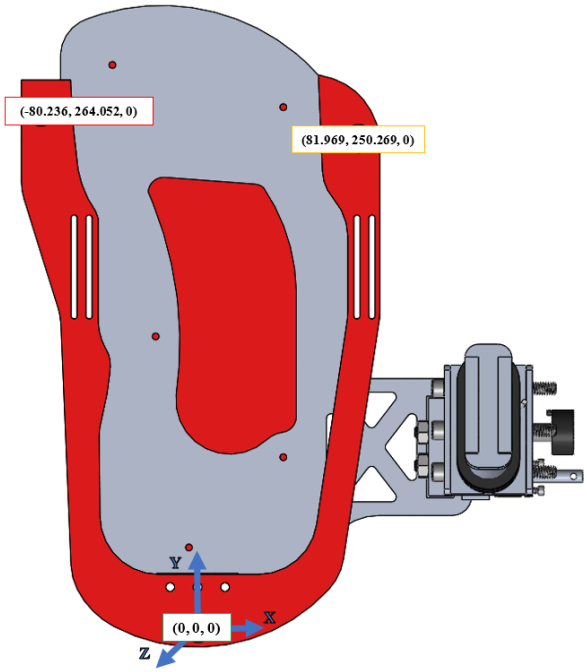

Figure 4.17: The positions of all three MOCAP markers as they would appear within the local reference frame of the AFO. Note that the origin is set at the position of the Heel Mocap Marker.

the "Toe-Down" position, the CoP point should be located between the two "Ball" FSRs, putting it the furthest away from the origin along the Y-Axis and slightly offsetting it along the X-Axis.

Using the recorded FSR values taken during the 3rd Iteration's trail 2, the AFO's local CoP point's position was calculated for the whole trial. The X, Y, and Z coordinates of the CoP position for this trial are shown in Figure 4.18, with the numerical values representing distance in mm. These results seem to follow the predicted behavior of the CoP position described above, with the X-coordinate position only changing when in the "Toe Down" position.

In order to verify that the program used to calculate the CoP on the AFO is working appropriately, though, these results needed to be compared to the independently calculated CoP data taken from the Vicon lab's own Force Plates. The

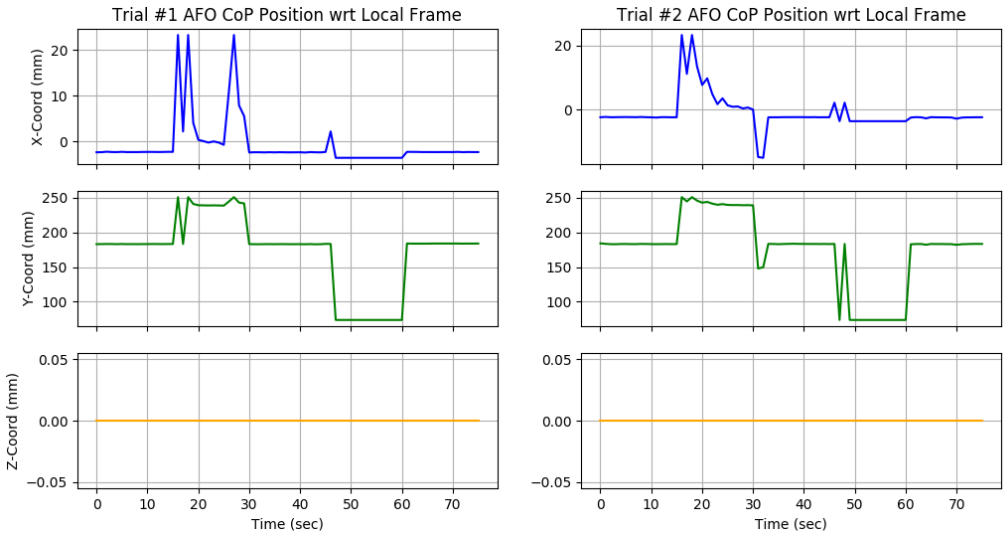

Figure 4.18: The Center-of-Pressure position coordinate data developed based off of solely the FSR readings during the 3rd version Sole-Sensor. The X-Y-Z positions listed here are in reference to the local coordinate frame of the AFO, not within the "world frame" of WPI's Vicon Lab.

Force-Plate's CoP values are calcated with respect to the "world frame", or the frame of reference of the VICON MOCAP Camera's within the WPI AIM Lab's Motion Capture room. Because these cameras take tens of thousands of data points over the course of trial's 76 seconds, a Linear Regression Fit was used to reduce the number of data points in order to match them with the AFO FSR values. These Linear-fitted Force-Plate values are shown in 4.19.

When comparing the AFO and Force-Plate CoP results from Figures 4.18 and 4.19, one trend in the data that becomes immediately apparent is how the Force-Plate's Y-Axis values seem to mirror the trend seen in the AFO's Y-Axis. This is due to how the AFO position was oriented within the World Reference frame when the test took place. As can be seen in Figure 4.20, the MOCAP markers attached to the AFO can be plotted within their respective positions in the world frame. By comparing the orientation of the markers in the world frame with their known positions in the AFO's local frame, it becomes clear that during the recording,

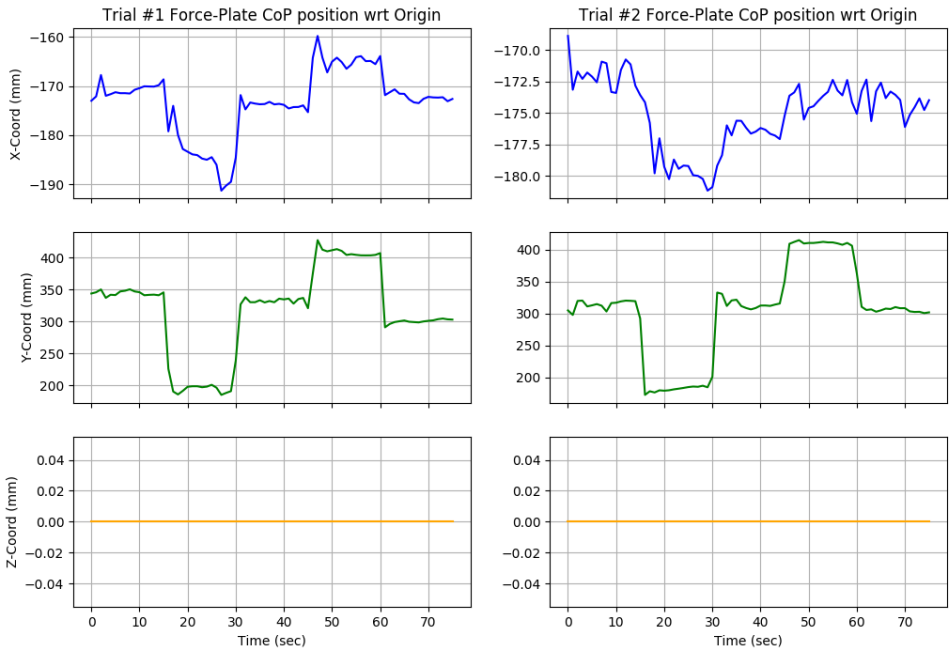

Figure 4.19: The Center-of-Pressure position coordinate data taken from the installed Force-Plates within the WPI AIM Lab's Vicon Motion-Capture room. These values have gone through a linear regression fit, so as to reduce the total number of individual data points from around $76,000$ to only 76 points. The X-Y-Z positions listed here are in reference to the "world frame" of WPI's Vicon Motion-Capture Room.

the AFO was located within the World-frame's 2nd quadrant (in the -X and +Y area). Furthermore, the AFO's local frame is also rotated some $+/-180°$ from the orientation of the world frame. Hence the reason why the Y-position data is essentially flipped between the two data sets: They both describe the same behavior, but in opposing reference frames.

Another trend of note is that the X-axis position data seems to vary much more greatly in the AFO than it does in the Force Plates. The exact reason for this is not fully known, though the range that the AFO's CoP moves across the X-axis, by $+/-20mm$, is what is expected based on the locations of the FSRs within the Sole-Sensor. As later analysis would shown, the discrepancy between the X-axis data would only become more evident once the two individual CoP points were properly

analyzed against with one another.

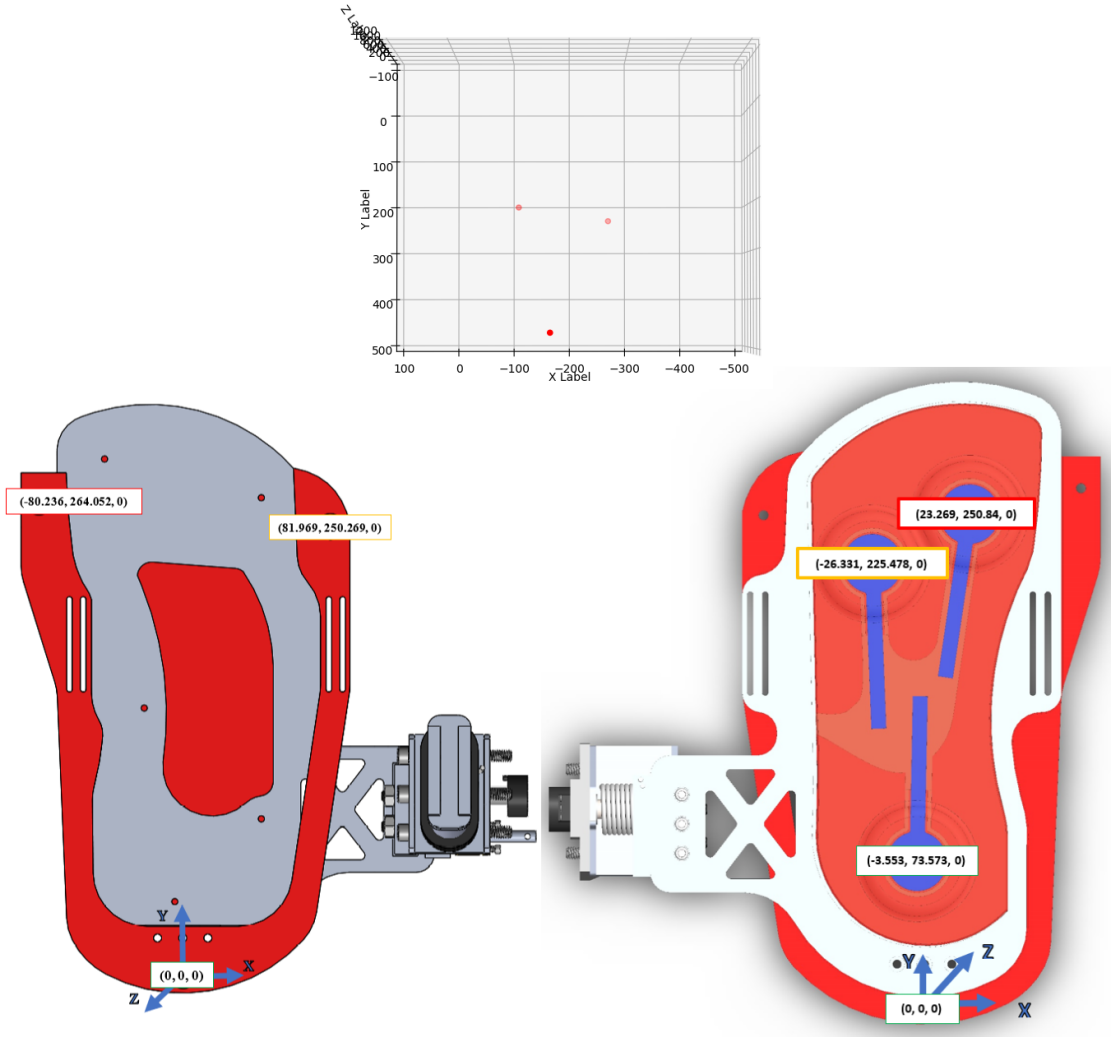

Figure 4.20: (Top) The positions of the VICON MOCAP markers as they appeared within the VICON environment when recording CoP data during the trails. (Bottom-Left) The positions of all three MOCAP markers as they would appear within the local reference frame of the AFO. Note that the origin is set at the position of the Heel Mocap Marker. (Bottom-Right)

In order to properly compare the CoP points between the AFO and the Force-Plates, a frame transformation taking into account both the Translation and Rotation of the AFO had to be conducted. Since the only indication of the AFO's position in the world frame comes from the recorded Motion-Capture Marker positions

taken during the trial, the transformation used was built around the methodology and scripts described by Nghia Ho to transform a set of points in 3D space from one coordinate frame to another [21]. Additionally, the code-base was built around the AIM-Vicon python library, developed by Nathaniel Goldfarb of the WPI Automative and Innovative Medicine lab, for running MOCAP-Marker motion-capture studies [22]. Taken together, this allowed us to translate the CoP from the AFO into the world reference frame based solely on the known positions of the MOCAP markers. The results of this successful transformation are shown below, in Figures 4.21 and 4.22. As can be seen in both figures, the AFO's Y-Axis CoP coordinate follows the same general trajectory with the Force-Plate's Y-coordinate, albeit slightly offset from one another. The same cannot be said for the X-axis values, however. While the X-coordinates do seem to follow a similar trend within Trial 1, it's evident that even with a successful frame transformation the AFO's CoP point travels a much greater distance across the X-axis than the Force-Plate's CoP does.

Additionally, it must be noted that in order to get the X-axis values to line up with each other at all during the transformation, the X-Coordinates of the individual FSRs had to have their signs flipped during the initial CoP calculation. This can be seen in the bottom-right figure of 4.20, where despite being flipped upside-down, the X-Axis arrow still points to the right such that both the Heel and Inner-Ball FSRs have negative X-coordinates. Doing this helps keep the AFO CoP's X-Coordinate values relatively in line with the Force-Plate after the transformation. This is especially evident in the CoP trajectory trails seen in Figure 4.22, wherein both AFO CoP trails drift to the same direction along the X-Axis as the Force-Plate trails.

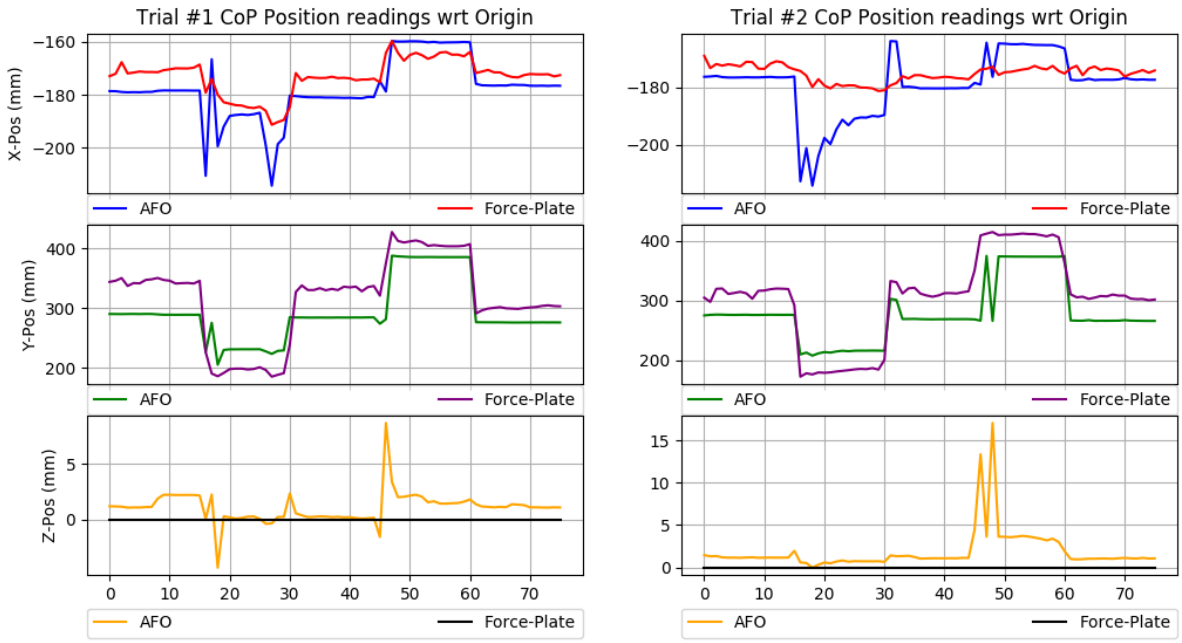

Figure 4.21: The CoP comparison results between the calculated AFO CoP point and the Force-Plate CoP point within the world frame, across both trials. Of note is that while Y-Coordinate values line up with each fairly well, the X-axis values show major discrepancies.

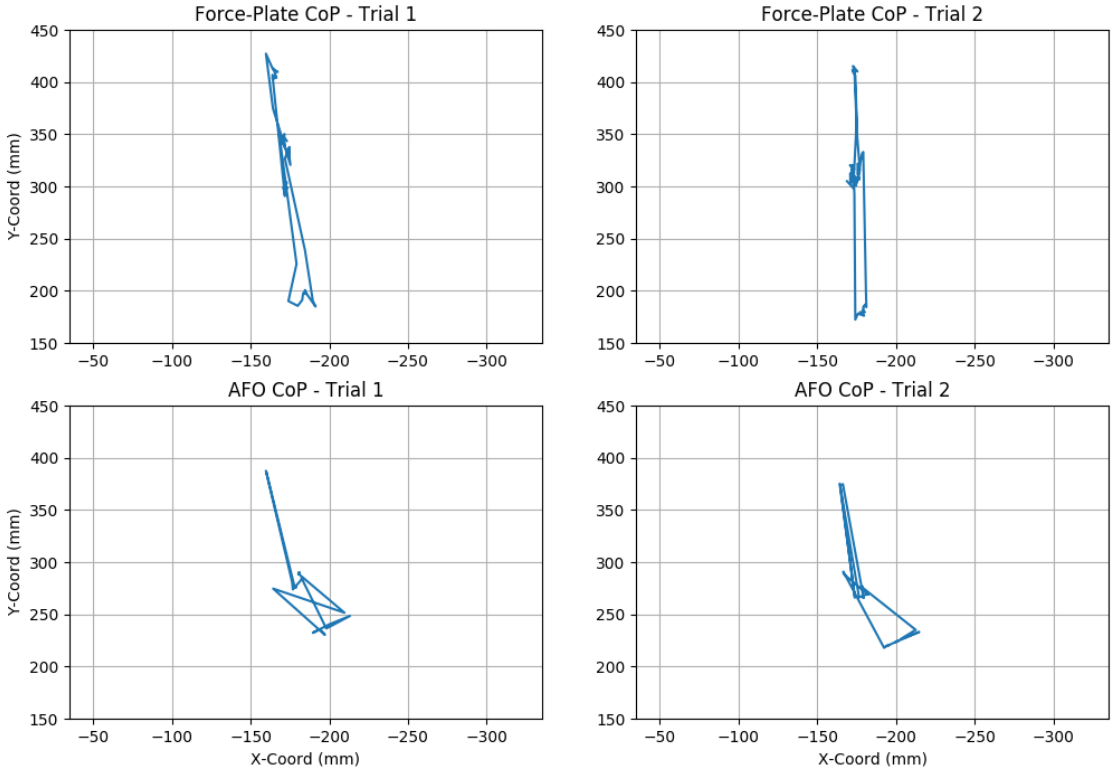

Figure 4.22: CoP Point trail created by both the Force-Plates and AFO across both trials. The shape created by the AFO point shows major distortions across the X-Axis when compared to their Force-Plate counterparts.

Chapter 5

Discussion

With this device, I have shown how Force-Sensing Resistor Sensors can be used within an AFO to not just to track the position of the foot, but to also calculate the distribution of Forces when the operator steps down. Using a combination of three FSRs, as opposed to only two like in [13], it becomes possible to detect not just when the foot is leaning forward or backward, but also when it is leaning to the sides. By reducing the raw FSR sensor values into being either "activated" or "non-activated", in a process known as "Binarization", each FSR can be treated as its own binary bit. This in turn allows for the creation of a 3-bit states diagram where the position of the AFO and the user's foot can be determined depending on which combination of FSRs are active at any point in time.

While binarizing the FSR values can be used to track foot position, doing the opposite and monitoring the magnitudes of the values returned allows the device to also track the concentration of forces from the foot, i.e. the Center-of-Pressure (CoP) point, comparing the magnitude of the values returned by the FSRs to their known positions within the AFO's local reference frame. The transformation of this point from the AFO local frame to the VICON Lab's "World" frame shows that it

roughly follows the trajectory of the independently calculated CoP point from the Force Plates, with the biggest discrepancy between the two values being a difference of $+/-3$cm along the X-axis and $+/-5$cm.

But while initial results with this project show promise, there were a number of additional tests that were originally planned but had to be cut due to current events. One such test is to record data from both the Sole-Sensor and the Potentiometer together within a single trial. Initial readings of the potentiometer sensor taken immediately after manufactured showed that the sensor did respond appropriately when rotating the joint. However, due to the unexpected amount of time needed to produce a working version of the Sole-Sensor, the actual values returned by the potentiometer were never parameterized into angular readings. One potential trial that can be done would be to have a user attach one of the AFO devices to their foot and walk around with it within the VICON motion capture room, unlike the prior test where the operator remained stationary on-top of the Force-Plates. Per each walking trial, data from both the potentiometer and the Sole-Sensor will be taken and used to help the L.A.R.R.E's main controller determine the actual Ankle-Joint orientation at any point in time.

Perhaps the most important test for this project, however, would be to run a series of trials that use both the Left and Right foot AFO systems together. The main purpose of the Sole-Sensor is to provide real-time sensory feedback in order to help the greater L.A.R.R.E system maintain its balance when in use, similar to systems seen in other robotic exoskeleton or humanoid robot systems. In order to do this, though, the L.A.R.R.E needs to know the position of its Center-of-Mass during normal walking gait, which requires having both AFO Sole-Sensors working in tandem with one another.

Appendix A

CAD

A.1 CAD Model Drawings

The following section contains the Machine-Part drawings needed to manufacture all the custom metal components that make up the Mechanical system of the AFO. Note that this section only includes the CAD for the Right-foot sub-assembly The components needed to make the Left-Foot AFO are almost exactly identical to their Right-Foot counterparts, except mirrored.

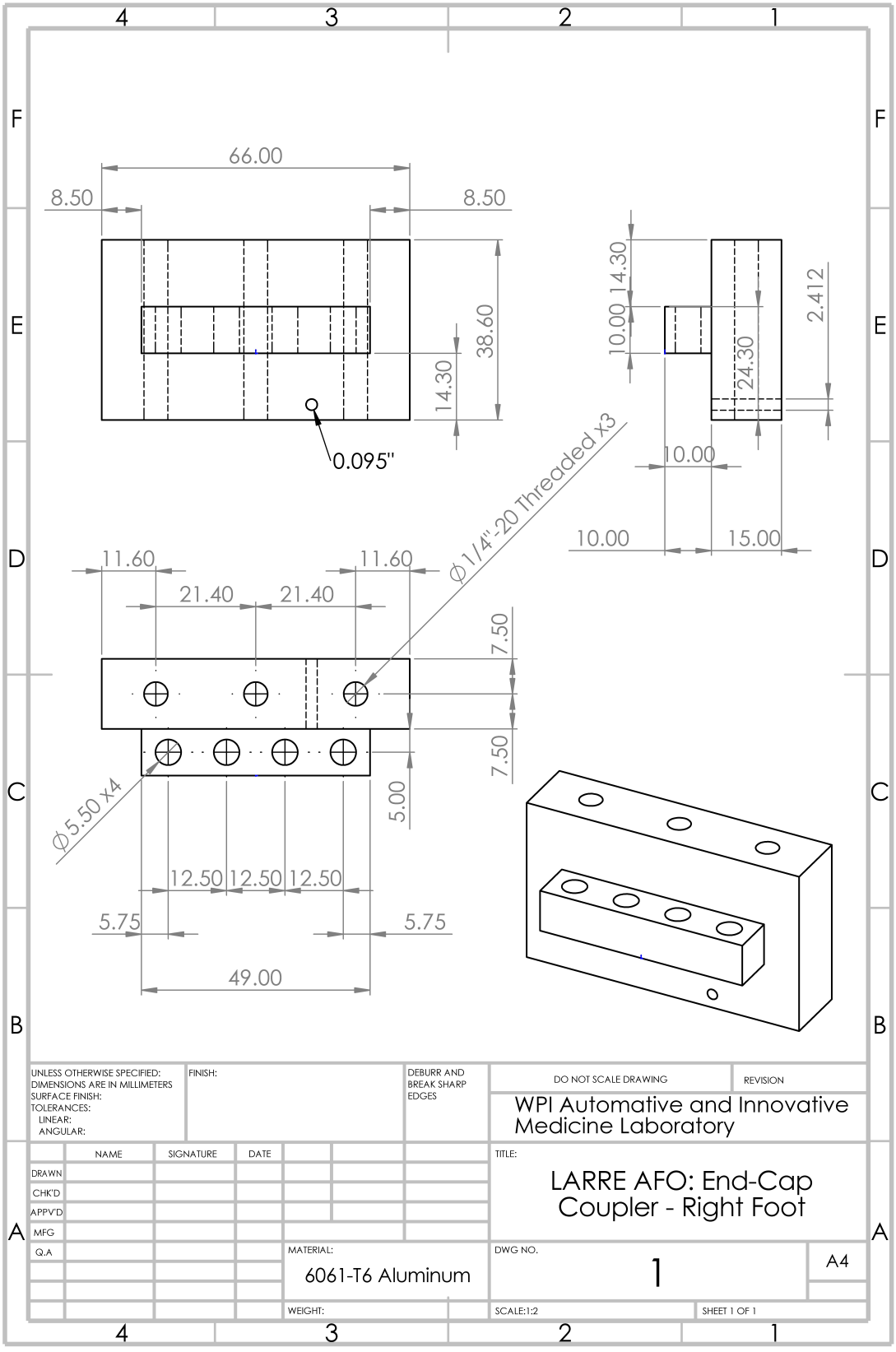
66.00
8.50
8.50
38.60
14.30
0.095"
14.30
10.00
2.412
24.30
10.00
10.00
15.00
Ø1/4"-20 Threaded x3
11.60
11.60
21.40
21.40
7.50
7.50
5.00
Ø5.50 x4
12.50
12.50
12.50
5.75
5.75
49.00
UNLESS OTHERWISE SPECIFIED:
DIMENSIONS ARE IN MILLIMETERS
SURFACE FINISH:
TOLERANCES:
LINEAR:
ANGULAR:
FINISH:
DEBURR AND BREAK SHARP EDGES
DO NOT SCALE DRAWING
REVISION
WPI Automative and Innovative Medicine Laboratory
NAME
SIGNATURE
DATE
DRAWN
CHK'D
APPV'D
MFG
Q.A
TITLE:
LARRE AFO: End-Cap Coupler - Right Foot
MATERIAL:
6061-T6 Aluminum
DWG NO.
1
A4
WEIGHT:
SCALE:1:2
SHEET 1 OF 1

Figure A.1

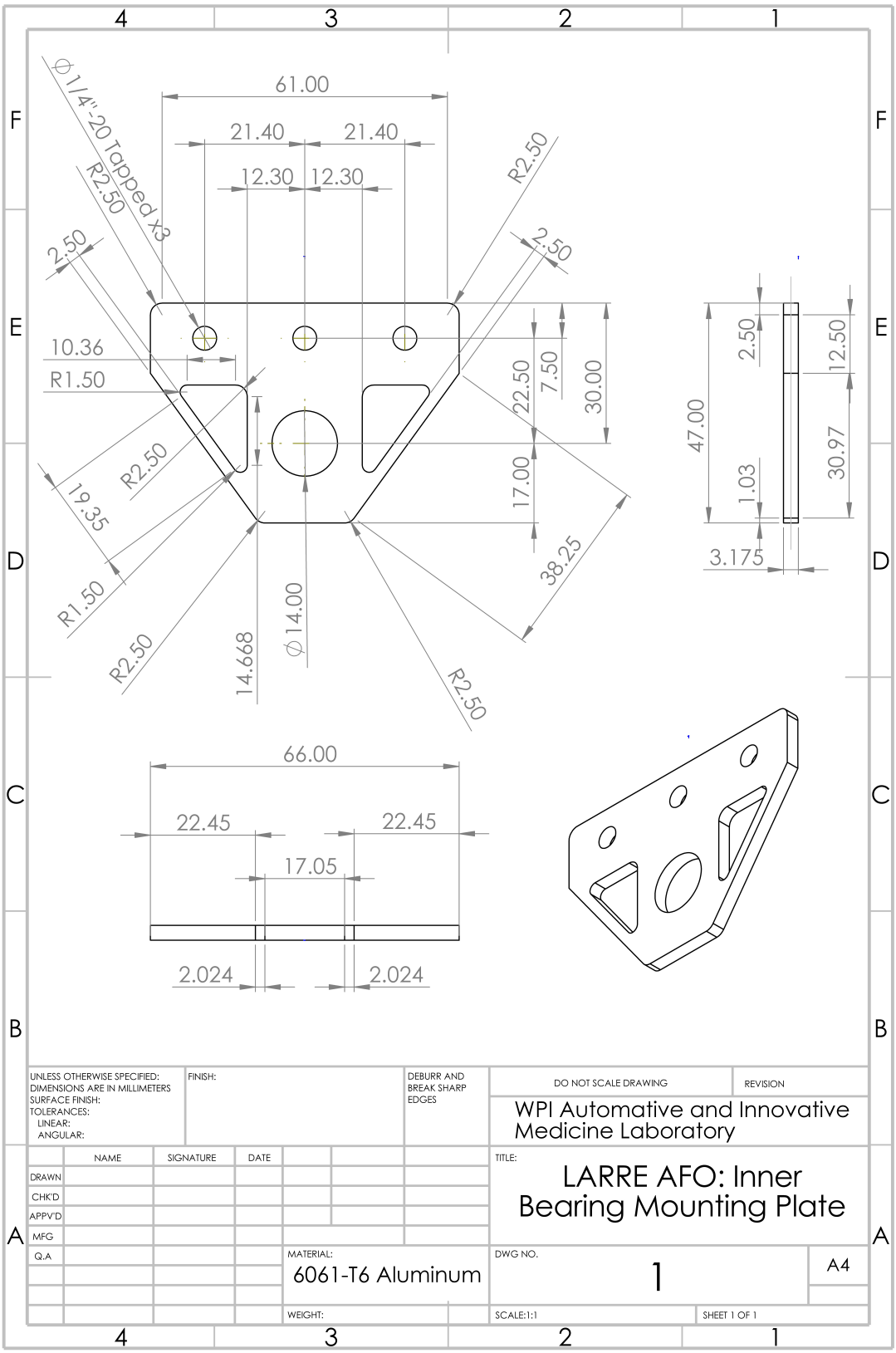
61.00
21.40
21.40
12.30
12.30
Ø1/4"-20 Tapped x3
R2.50
R2.50
2.50
2.50
10.36
R1.50
R2.50
19.35
R1.50
R2.50
14.668
Ø14.00
R2.50
22.50
7.50
30.00
17.00
38.25
2.50
12.50
47.00
30.97
1.03
3.175
66.00
22.45
22.45
17.05
2.024
2.024
UNLESS OTHERWISE SPECIFIED:
DIMENSIONS ARE IN MILLIMETERS
SURFACE FINISH:
TOLERANCES:
LINEAR:
ANGULAR:
FINISH:
DEBURR AND BREAK SHARP EDGES
DO NOT SCALE DRAWING
REVISION
WPI Automative and Innovative Medicine Laboratory
NAME
SIGNATURE
DATE
DRAWN
CHK'D
APPV'D
MFG
Q.A
TITLE:
LARRE AFO: Inner Bearing Mounting Plate
MATERIAL:
6061-T6 Aluminum
DWG NO.
1
A4
WEIGHT:
SCALE:1:1
SHEET 1 OF 1

Figure A.2

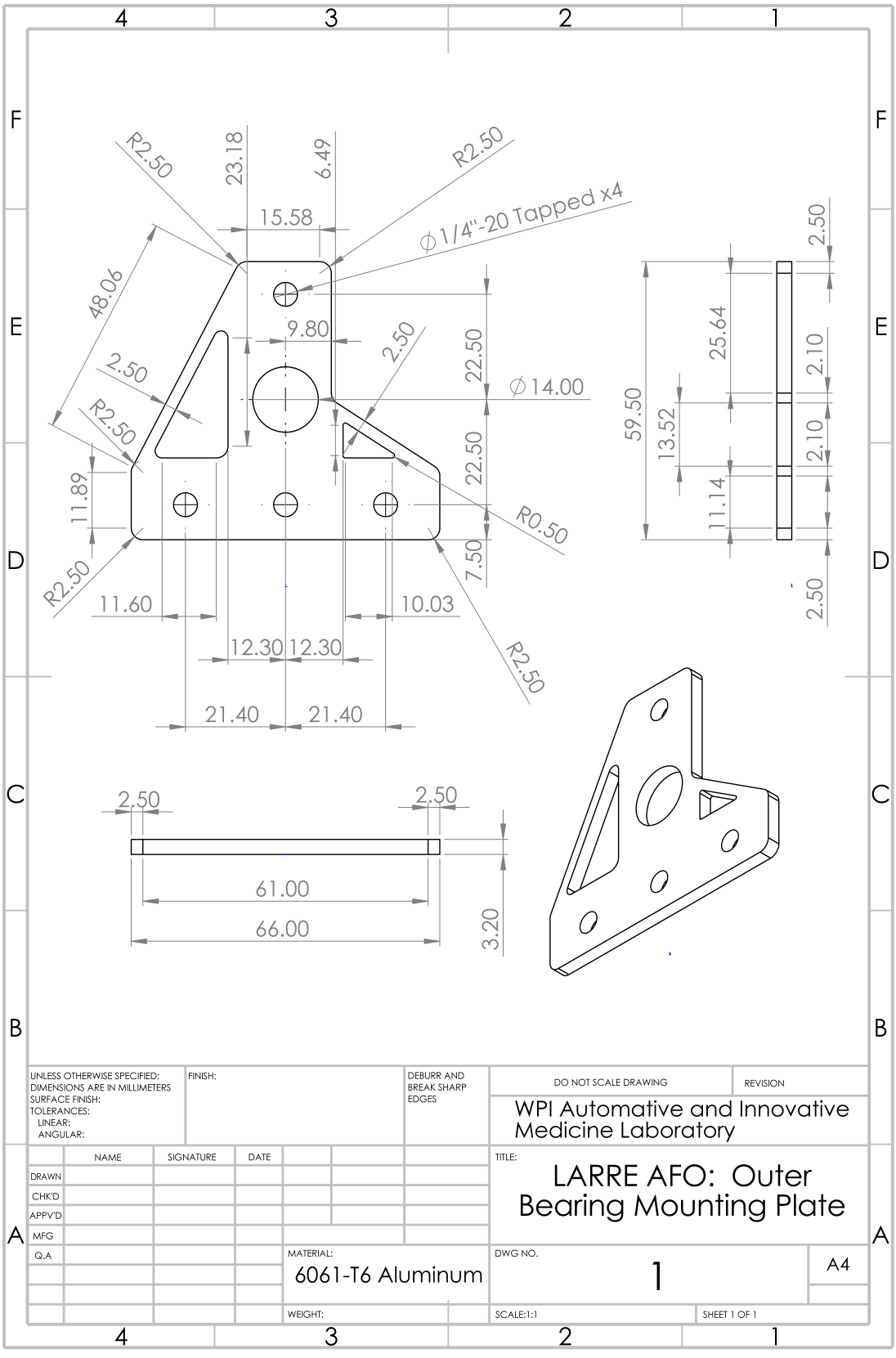
R2.50
23.18
6.49
R2.50
15.58
⌀1/4"-20 Tapped x4
48.06
9.80
2.50
22.50
⌀14.00
2.50
R2.50
22.50
11.89
R0.50
R2.50
7.50
11.60
10.03
12.30 12.30
R2.50
21.40 21.40
2.50
25.64
2.10
59.50
13.52
2.10
11.14
2.50
2.50
2.50
61.00
66.00
3.20
UNLESS OTHERWISE SPECIFIED:
DIMENSIONS ARE IN MILLIMETERS
SURFACE FINISH:
TOLERANCES:
LINEAR:
ANGULAR:
FINISH:
DEBURR AND BREAK SHARP EDGES
DO NOT SCALE DRAWING
REVISION
WPI Automative and Innovative Medicine Laboratory
NAME
SIGNATURE
DATE
DRAWN
CHK'D
APPV'D
MFG
Q.A
TITLE:
LARRE AFO: Outer Bearing Mounting Plate
MATERIAL:
6061-T6 Aluminum
DWG NO.
1
A4
WEIGHT:
SCALE:1:1
SHEET 1 OF 1

Figure A.3

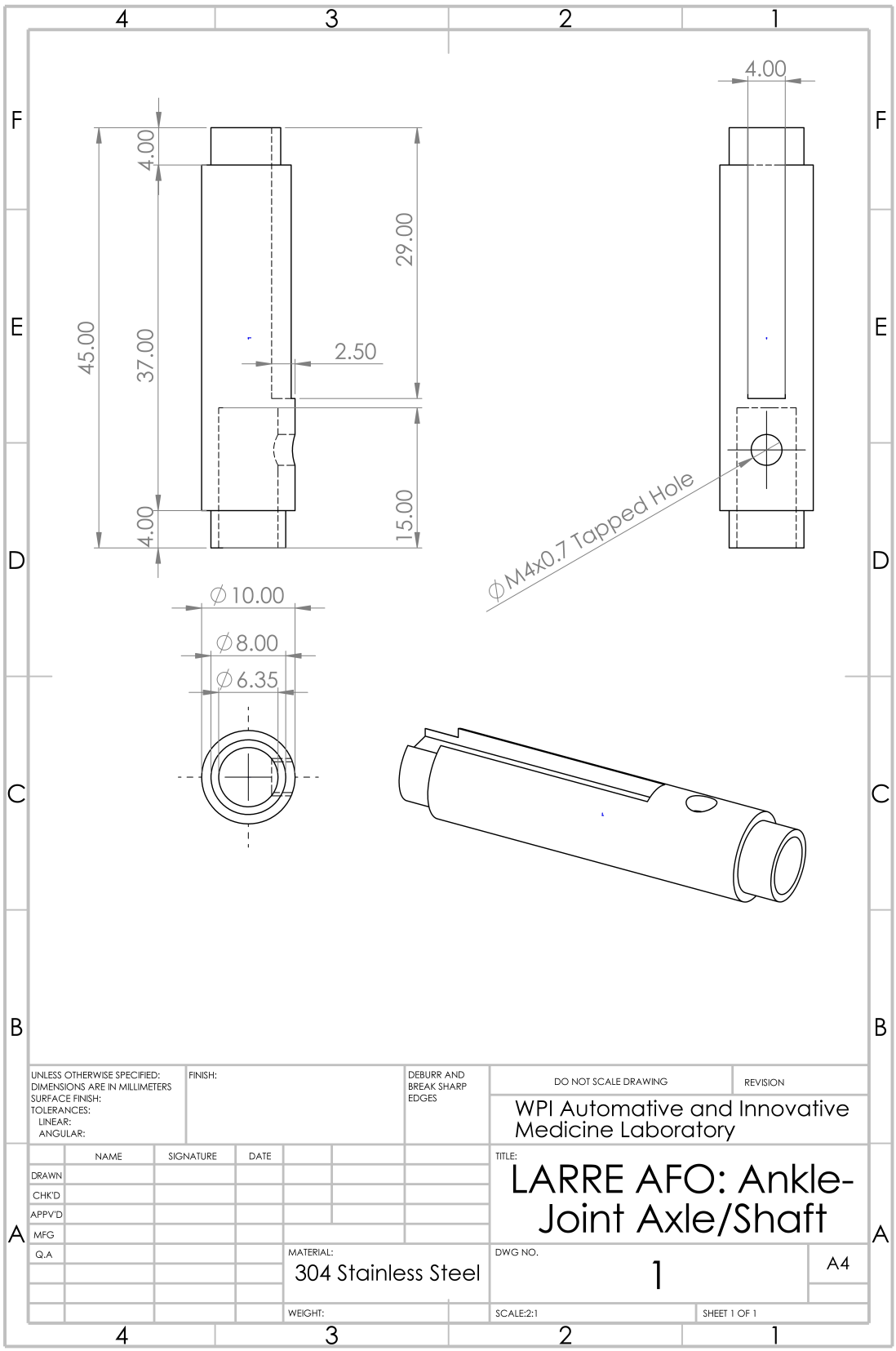
4.00
4.00
29.00
45.00
37.00
2.50
4.00
15.00
∅M4x0.7 Tapped Hole
∅10.00
∅8.00
∅6.35
UNLESS OTHERWISE SPECIFIED:
DIMENSIONS ARE IN MILLIMETERS
SURFACE FINISH:
TOLERANCES:
LINEAR:
ANGULAR:
FINISH:
DEBURR AND BREAK SHARP EDGES
DO NOT SCALE DRAWING
REVISION
WPI Automative and Innovative Medicine Laboratory
NAME
SIGNATURE
DATE
DRAWN
CHK'D
APPV'D
MFG
Q.A
TITLE:
LARRE AFO: Ankle-Joint Axle/Shaft
MATERIAL:
304 Stainless Steel
DWG NO.
1
A4
WEIGHT:
SCALE:2:1
SHEET 1 OF 1

Figure A.4

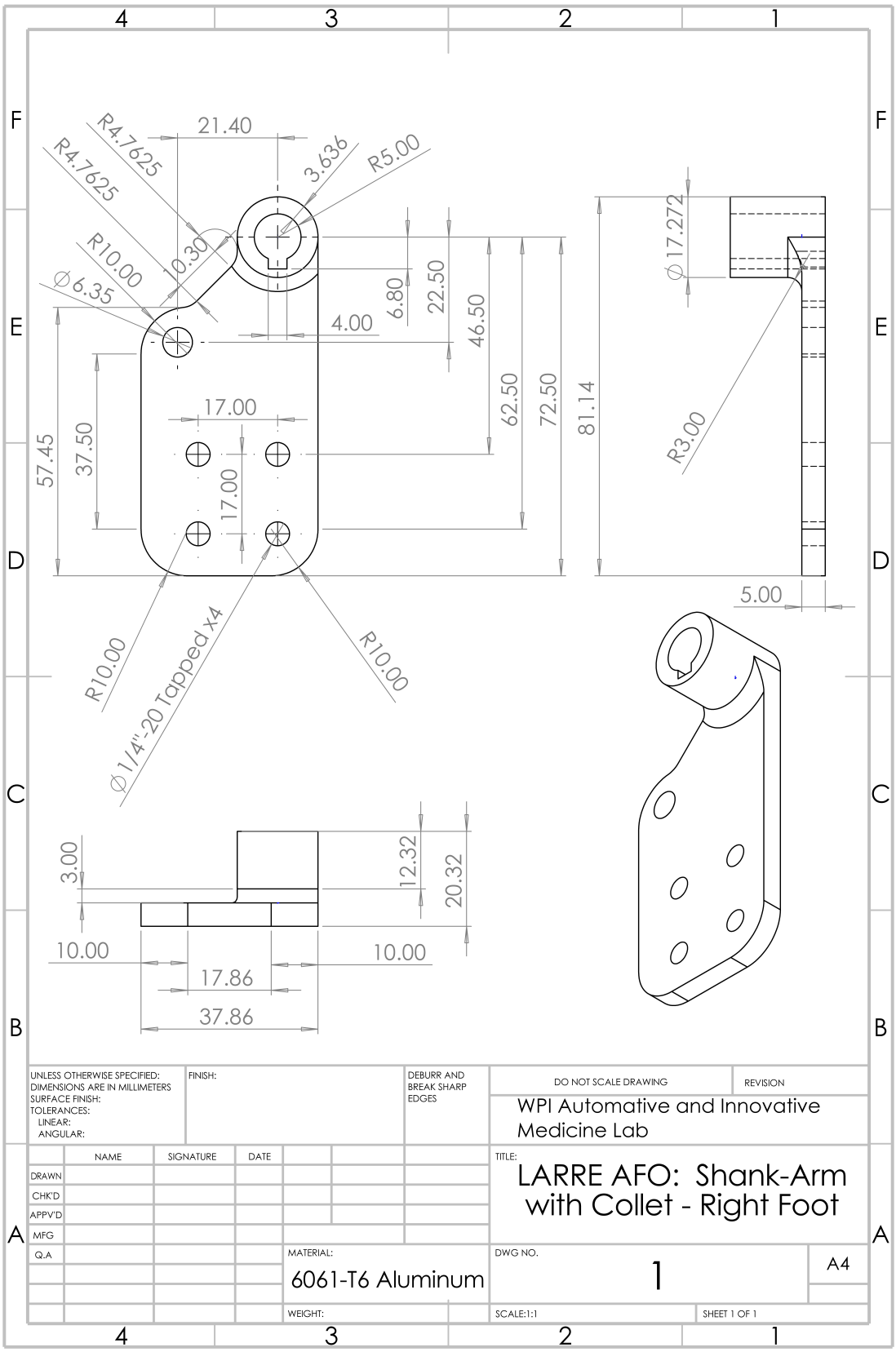
21.40
R4.7625
R4.7625
3.636
R5.00
R10.00
10.30
⌀6.35
4.00
6.80
22.50
46.50
62.50
72.50
57.45
37.50
17.00
17.00
81.14
⌀17.272
R3.00
5.00
R10.00
⌀1/4"-20 Tapped x4
R10.00
3.00
12.32
20.32
10.00
17.86
10.00
37.86
UNLESS OTHERWISE SPECIFIED:
DIMENSIONS ARE IN MILLIMETERS
SURFACE FINISH:
TOLERANCES:
LINEAR:
ANGULAR:
FINISH:
DEBURR AND BREAK SHARP EDGES
DO NOT SCALE DRAWING
REVISION
WPI Automative and Innovative Medicine Lab
NAME
SIGNATURE
DATE
DRAWN
CHK'D
APPV'D
MFG
Q.A
TITLE:
LARRE AFO: Shank-Arm with Collet - Right Foot
MATERIAL:
6061-T6 Aluminum
DWG NO.
1
A4
WEIGHT:
SCALE:1:1
SHEET 1 OF 1

Figure A.5

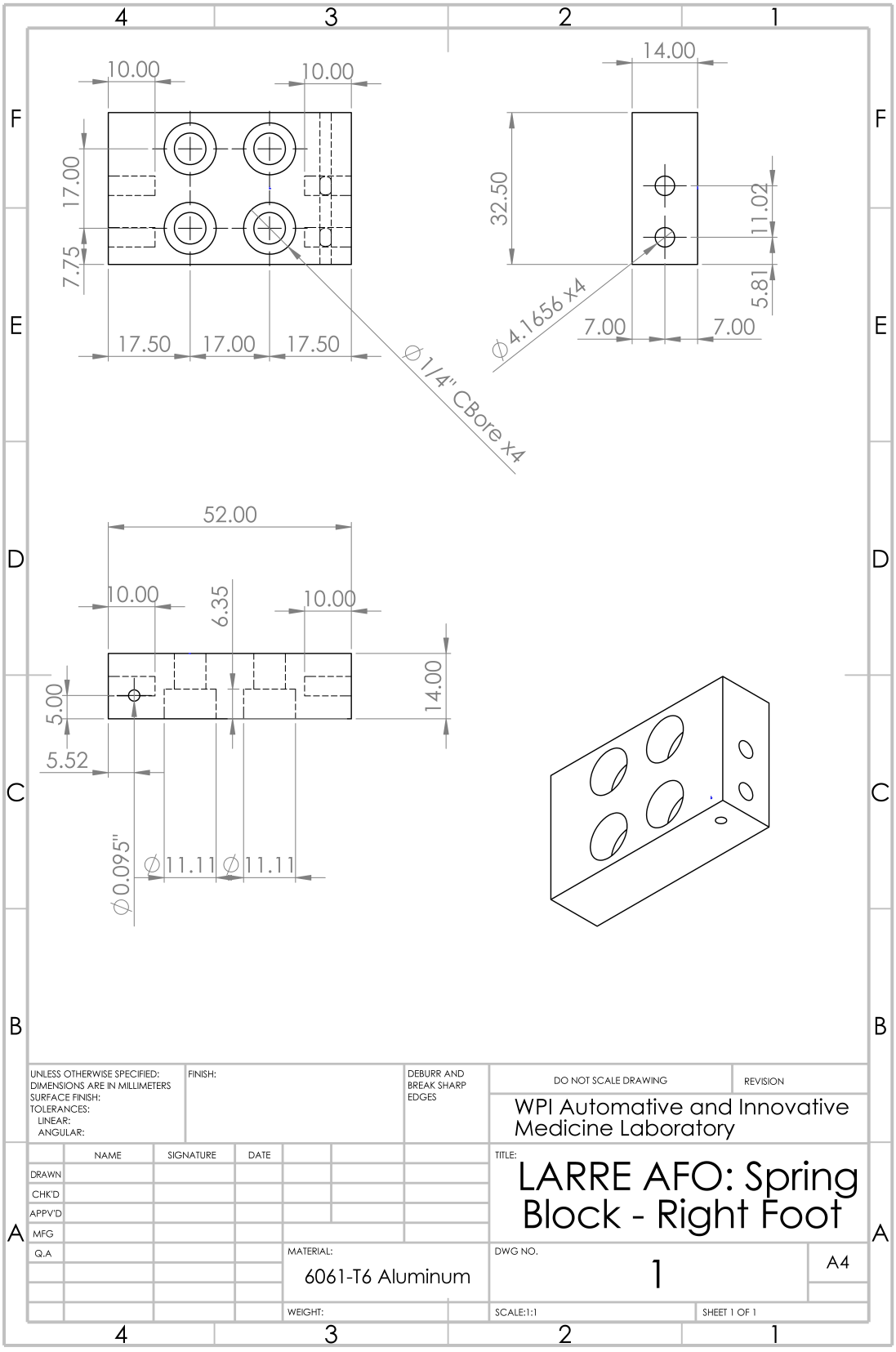
10.00
10.00
17.00
7.75
17.50
17.00
17.50
Ø1/4" CBore x4
14.00
32.50
11.02
5.81
Ø4.1656 x4
7.00
7.00
52.00
10.00
6.35
10.00
14.00
5.00
5.52
Ø0.095"
Ø11.11
Ø11.11
UNLESS OTHERWISE SPECIFIED:
DIMENSIONS ARE IN MILLIMETERS
SURFACE FINISH:
TOLERANCES:
LINEAR:
ANGULAR:
FINISH:
DEBURR AND BREAK SHARP EDGES
DO NOT SCALE DRAWING
REVISION
WPI Automative and Innovative Medicine Laboratory
NAME
SIGNATURE
DATE
DRAWN
CHK'D
APPV'D
MFG
Q.A
TITLE:
LARRE AFO: Spring Block - Right Foot
MATERIAL:
6061-T6 Aluminum
DWG NO.
1
A4
WEIGHT:
SCALE:1:1
SHEET 1 OF 1

Figure A.6

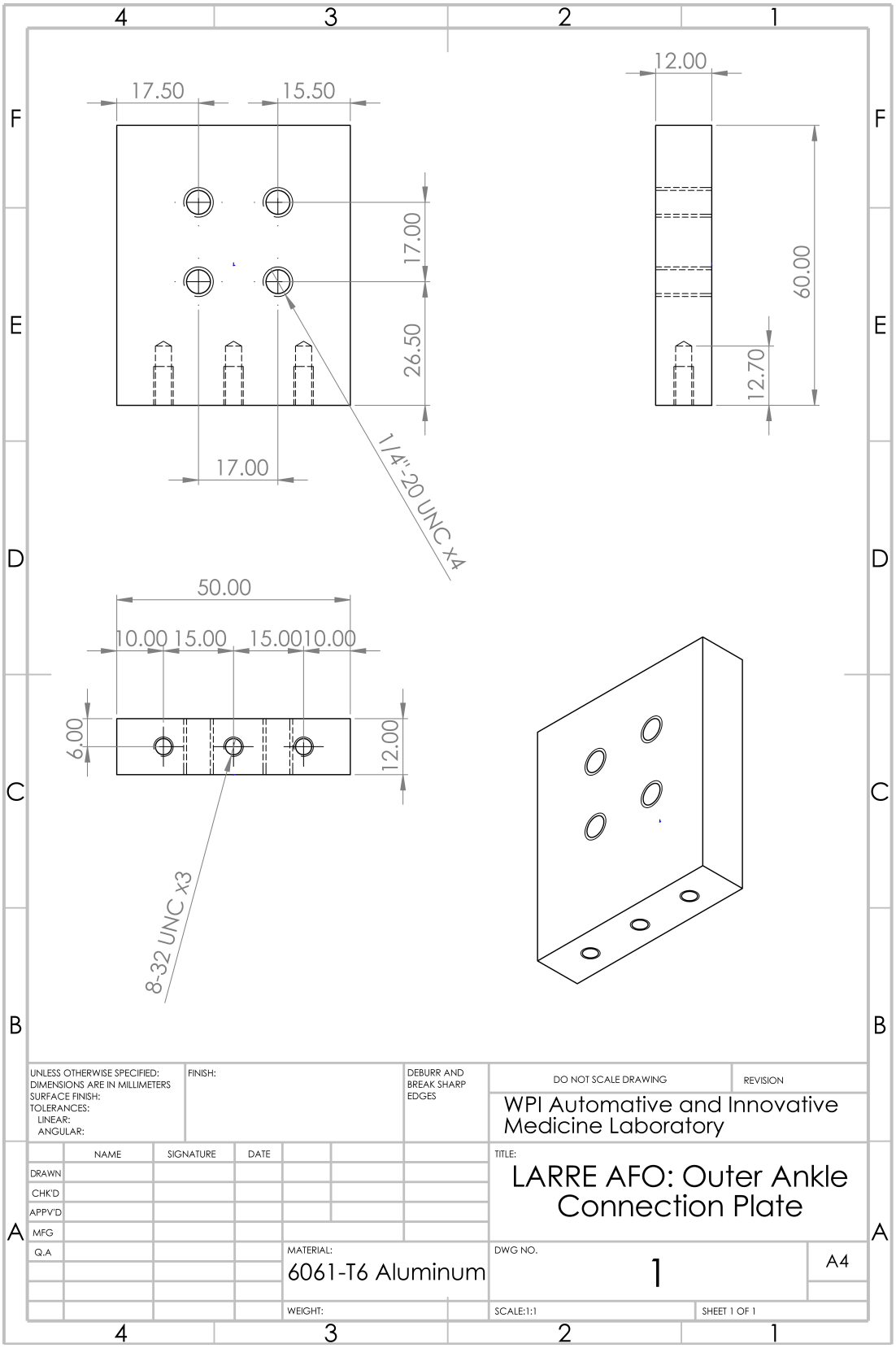
17.50
15.50
17.00
26.50
17.00
1/4"-20 UNC x4
12.00
60.00
12.70
50.00
10.00 15.00 15.00 10.00
6.00
12.00
8-32 UNC x3
UNLESS OTHERWISE SPECIFIED:
DIMENSIONS ARE IN MILLIMETERS
SURFACE FINISH:
TOLERANCES:
LINEAR:
ANGULAR:
FINISH:
DEBURR AND BREAK SHARP EDGES
DO NOT SCALE DRAWING
REVISION
WPI Automative and Innovative Medicine Laboratory
NAME
SIGNATURE
DATE
DRAWN
CHK'D
APPV'D
MFG
Q.A
TITLE:
LARRE AFO: Outer Ankle Connection Plate
MATERIAL:
6061-T6 Aluminum
DWG NO.
1
A4
WEIGHT:
SCALE:1:1
SHEET 1 OF 1

Figure A.7

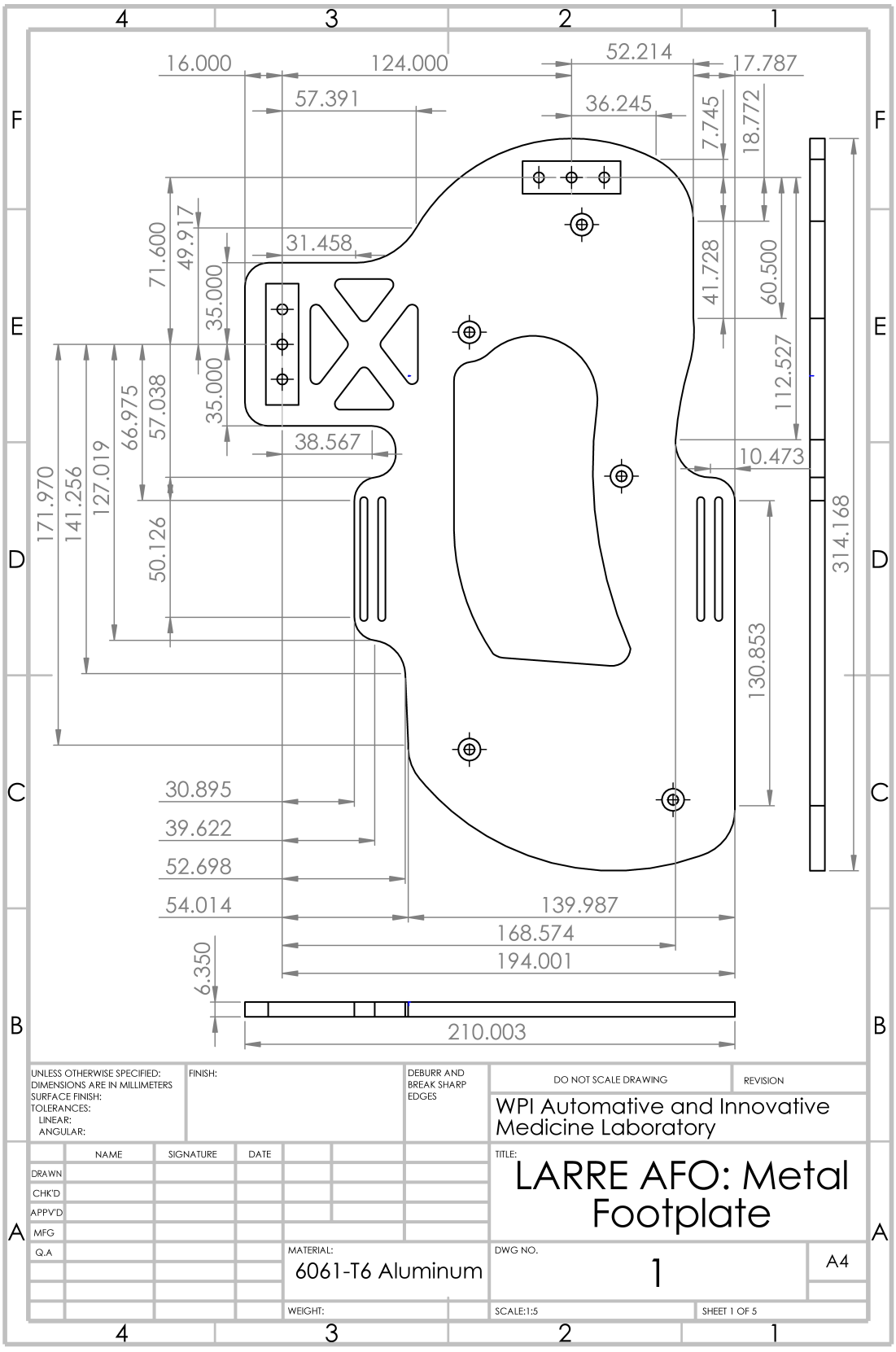
16.000
124.000
52.214
17.787
57.391
36.245
7.745
18.772
71.600
49.917
31.458
41.728
60.500
35.000
35.000
112.527
66.975
57.038
38.567
10.473
171.970
141.256
127.019
50.126
314.168
130.853
30.895
39.622
52.698
54.014
139.987
168.574
194.001
6.350
210.003
UNLESS OTHERWISE SPECIFIED:
DIMENSIONS ARE IN MILLIMETERS
SURFACE FINISH:
TOLERANCES:
LINEAR:
ANGULAR:
FINISH:
DEBURR AND BREAK SHARP EDGES
DO NOT SCALE DRAWING
REVISION
WPI Automative and Innovative Medicine Laboratory
NAME
SIGNATURE
DATE
DRAWN
CHK'D
APPV'D
MFG
Q.A
TITLE:
LARRE AFO: Metal Footplate
MATERIAL:
6061-T6 Aluminum
DWG NO.
1
A4
WEIGHT:
SCALE:1:5
SHEET 1 OF 5

Figure A.8

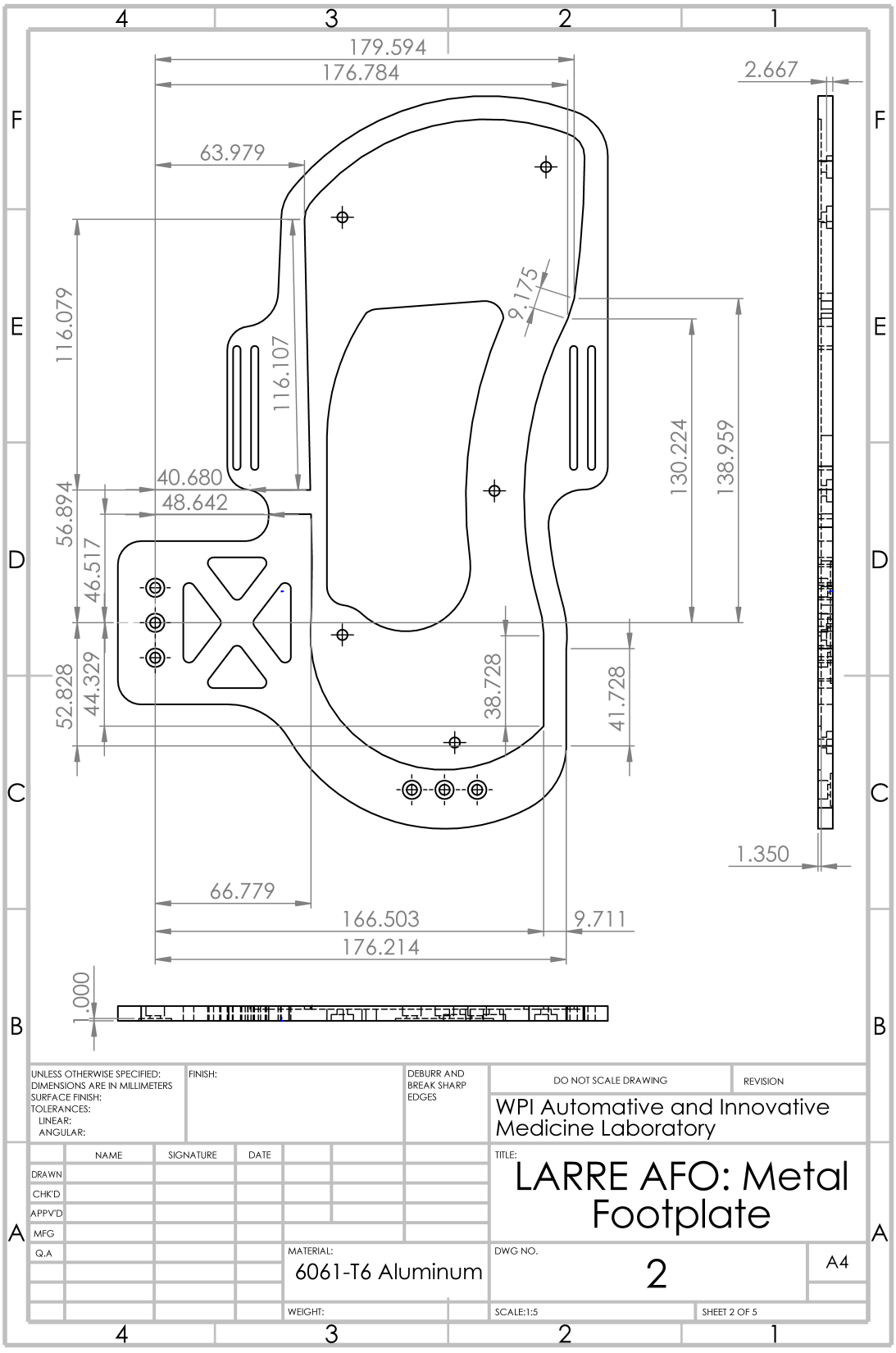
179.594
176.784
2.667
63.979
116.079
116.107
9.175
130.224
138.959
40.680
48.642
56.894
46.517
52.828
44.329
38.728
41.728
1.350
66.779
166.503
176.214
9.711
1.000
UNLESS OTHERWISE SPECIFIED:
DIMENSIONS ARE IN MILLIMETERS
SURFACE FINISH:
TOLERANCES:
LINEAR:
ANGULAR:
FINISH:
DEBURR AND BREAK SHARP EDGES
DO NOT SCALE DRAWING
REVISION
WPI Automative and Innovative Medicine Laboratory
NAME
SIGNATURE
DATE
DRAWN
CHK'D
APPV'D
MFG
Q.A
TITLE:
LARRE AFO: Metal Footplate
MATERIAL:
6061-T6 Aluminum
DWG NO.
2
A4
WEIGHT:
SCALE:1:5
SHEET 2 OF 5

Figure A.9

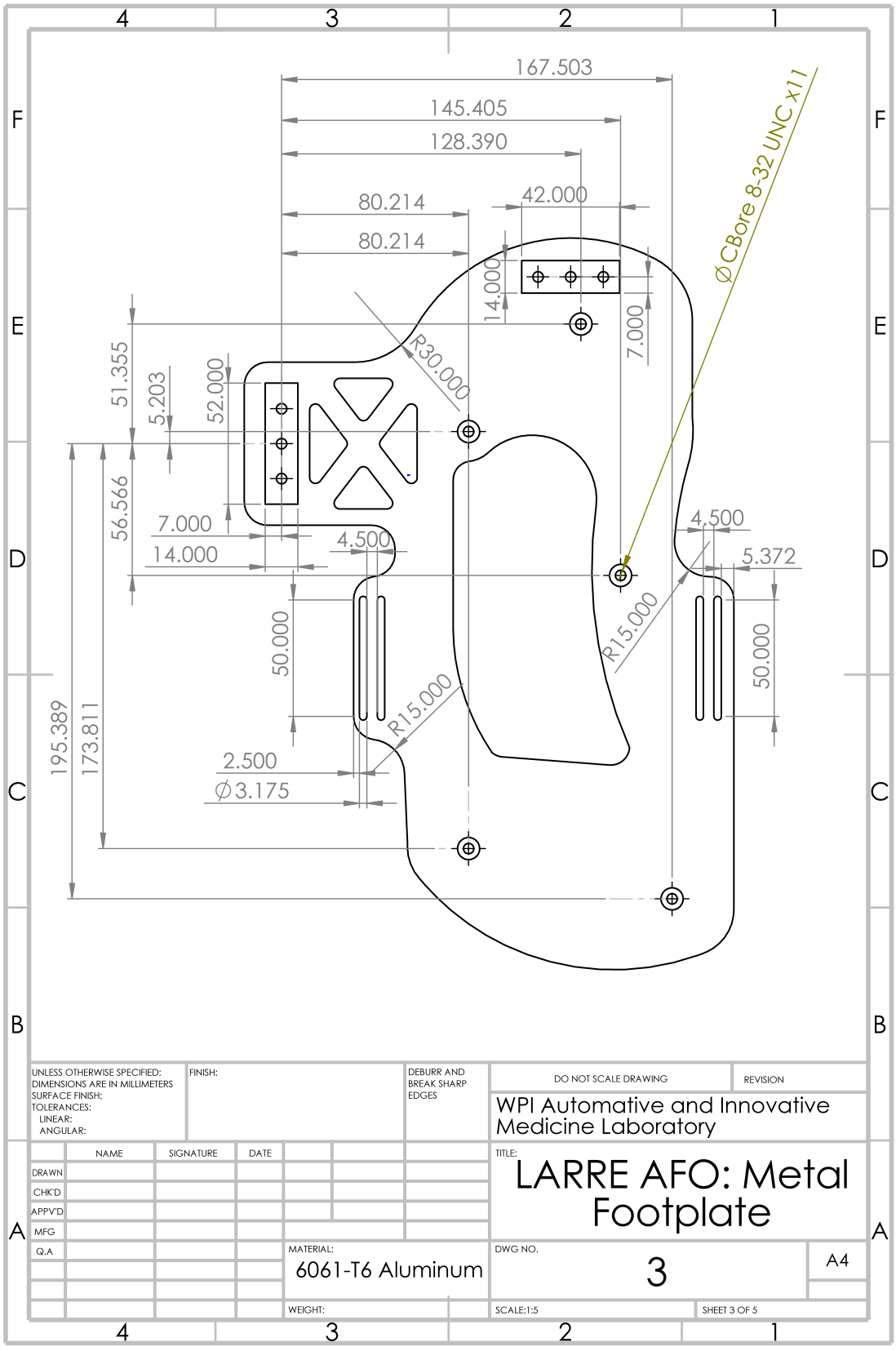
167.503
145.405
128.390
80.214
80.214
42.000
Ø CBore 8-32 UNC x11
14.000
7.000
R30.000
51.355
5.203
52.000
56.566
7.000
14.000
4.500
4.500
5.372
50.000
R15.000
50.000
R15.000
195.389
173.811
2.500
Ø3.175
4
3
2
1
F
E
D
C
B
A
UNLESS OTHERWISE SPECIFIED:
DIMENSIONS ARE IN MILLIMETERS
SURFACE FINISH:
TOLERANCES:
LINEAR:
ANGULAR:
FINISH:
DEBURR AND BREAK SHARP EDGES
DO NOT SCALE DRAWING
REVISION
WPI Automative and Innovative Medicine Laboratory
NAME
SIGNATURE
DATE
DRAWN
CHK'D
APPV'D
MFG
Q.A
TITLE:
LARRE AFO: Metal Footplate
MATERIAL:
6061-T6 Aluminum
DWG NO.
3
A4
WEIGHT:
SCALE:1:5
SHEET 3 OF 5

Figure A.10

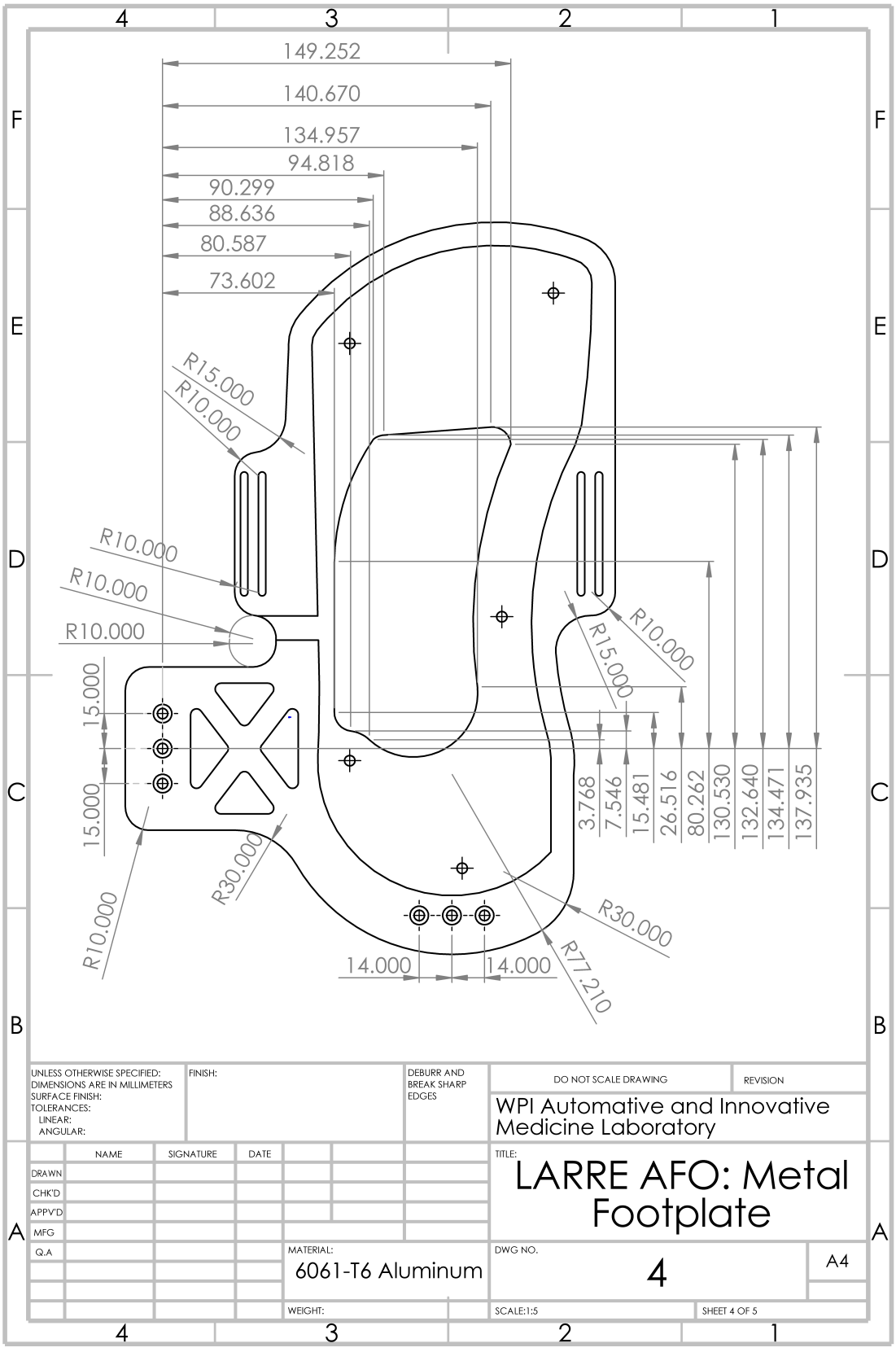
149.252
140.670
134.957
94.818
90.299
88.636
80.587
73.602
R15.000
R10.000
R10.000
R10.000
R10.000
R15.000
R10.000
15.000
15.000
3.768
7.546
15.481
26.516
80.262
130.530
132.640
134.471
137.935
R30.000
R10.000
R30.000
R77.210
14.000
14.000
UNLESS OTHERWISE SPECIFIED:
DIMENSIONS ARE IN MILLIMETERS
SURFACE FINISH:
TOLERANCES:
LINEAR:
ANGULAR:
FINISH:
DEBURR AND BREAK SHARP EDGES
DO NOT SCALE DRAWING
REVISION
WPI Automative and Innovative Medicine Laboratory
NAME
SIGNATURE
DATE
DRAWN
CHK'D
APPV'D
MFG
Q.A
TITLE:
LARRE AFO: Metal Footplate
MATERIAL:
6061-T6 Aluminum
DWG NO.
4
A4
WEIGHT:
SCALE:1:5
SHEET 4 OF 5

Figure A.11

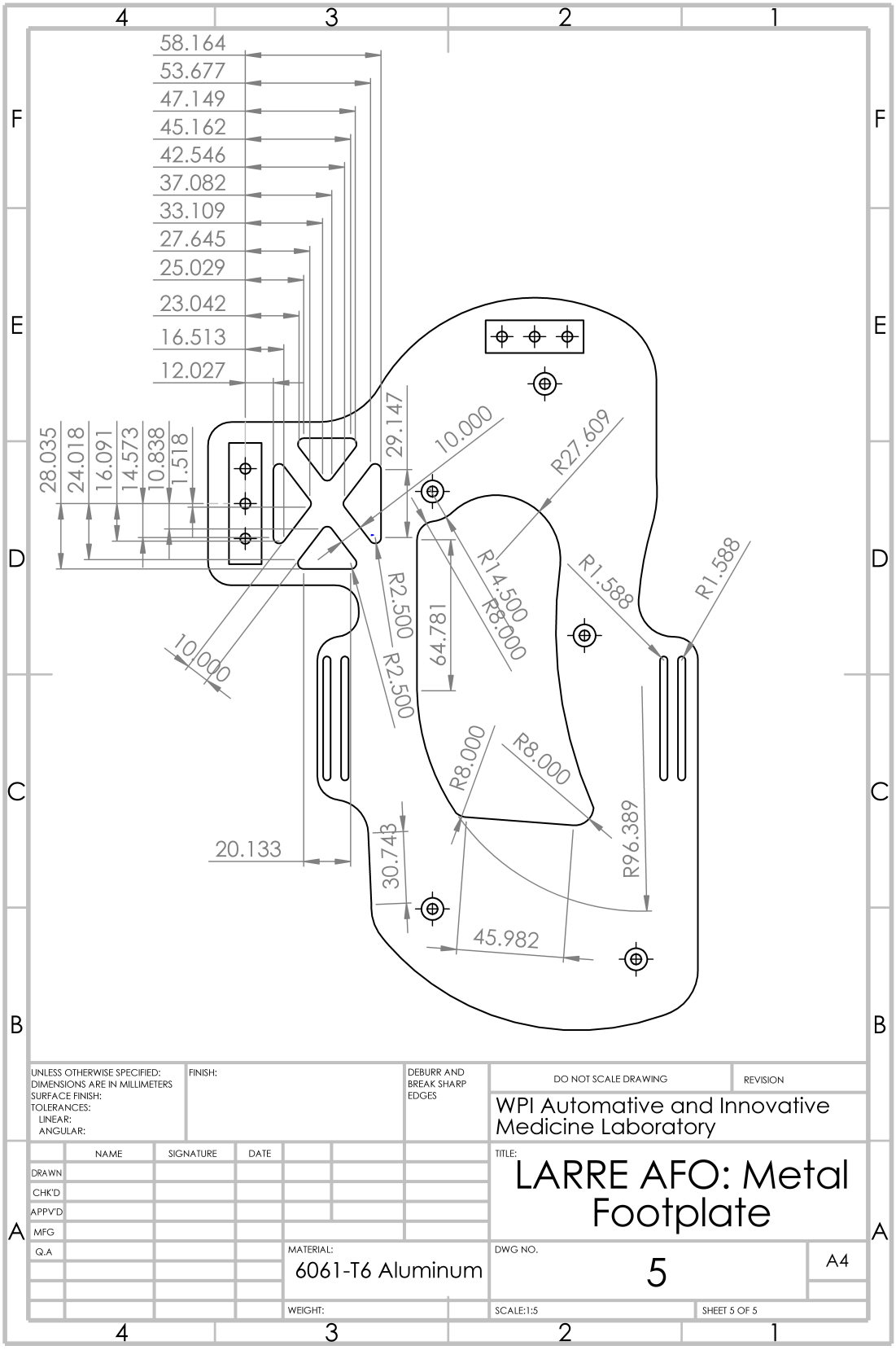
58.164
53.677
47.149
45.162
42.546
37.082
33.109
27.645
25.029
23.042
16.513
12.027
28.035
24.018
16.091
14.573
10.838
1.518
29.147
10.000
R27.609
R14.500
R8.000
R1.588
R1.588
R2.500
R2.500
64.781
10.000
R8.000
R8.000
R96.389
20.133
30.743
45.982
UNLESS OTHERWISE SPECIFIED:
DIMENSIONS ARE IN MILLIMETERS
SURFACE FINISH:
TOLERANCES:
LINEAR:
ANGULAR:
FINISH:
DEBURR AND BREAK SHARP EDGES
DO NOT SCALE DRAWING
REVISION
WPI Automative and Innovative Medicine Laboratory
NAME
SIGNATURE
DATE
DRAWN
CHK'D
APPV'D
MFG
Q.A
TITLE:
LARRE AFO: Metal Footplate
MATERIAL:
6061-T6 Aluminum
DWG NO.
5
A4
WEIGHT:
SCALE:1:5
SHEET 5 OF 5

Figure A.12

Appendix B

Tables

B.1 Material Properties Tables

This section contains the material properties tables of the materials of the components run through the FEA Static Simulations.

6061-T6 Aluminum Alloy		
Property	Value	Units
Elastic Modulus	69	GPa
Poisson's Ratio	0.33	N/A
Shear Modulus	26	GPa
Mass Density	2700	kg/m^3
Tensile Strength	0.31	GPa
Compressive Strength	0.31	GPa
Yield Strength	0.275	GPa

Table B.1: 6061 $T6$ Aluminum Alloy Material Properties Table

AISI 304 Stainless Steel Alloy		
Property	Value	Units
Elastic Modulus	190	GPa
Poisson's Ratio	0.29	N/A
Shear Modulus	75	GPa
Mass Density	8000	kg/m^3
Tensile Strength	0.517	GPa
Compressive Strength	0.517	GPa
Yield Strength	0.2068	GPa

Table B.2: AISI 304 Stainless Steel Alloy Material Properties Table

Bibliography

[1] T. Seymour and W. Morrison, "Medical news today: How to improve poor dorsiflexion," 08 2017.

[2] "Alimed afo info blog."

[3] "Webmd: Foot drop condition definition."

[4] Y. Bai, F. Li, J. Zhao, J. Li, F. Jin, and X. Gao, "A powered ankle-foot orthoses for ankle rehabilitation," in *2012 IEEE International Conference on Automation and Logistics*, pp. 288–293, Aug 2012.

[5] G. Gomes, I. Lourenço, J. Oliveira, M. Gomes, A. Vale, L. Freire, P. Quental, H. Policarpo, and J. Matos, "Structural reinforcements on afo's: A study using computer-aided design and finite element method," in *2017 IEEE 5th Portuguese Meeting on Bioengineering (ENBENG)*, pp. 1–4, 2017.

[6] Y. Zhang, R. J. Kleinmann, K. J. Nolan, and D. Zanotto, "Preliminary validation of a cable-driven powered ankle–foot orthosis with dual actuation mode," *IEEE Transactions on Medical Robotics and Bionics*, vol. 1, no. 1, pp. 30–37, 2019.

[7] J. Chern, H. Chang, C. Lung, C. Wu, and S. F. Tang, "Static ankle-foot orthosis improves static balance and gait functions in hemiplegic patients after stroke," in *2013 35th Annual International Conference of the IEEE Engineering in Medicine and Biology Society (EMBC)*, pp. 5009–5012, July 2013.

[8] E. Russell Esposito, K. A. Schmidtbauer, and J. M. Wilken, "Experimental comparisons of passive and powered ankle-foot orthoses in individuals with limb reconstruction," *Journal of NeuroEngineering and Rehabilitation*, vol. 15, no. 1, p. 111, 2018.

[9] N. Yoshizawa, "Active afo with ankle joint brake friction control using force observer," September 2012.

[10] R. Chin, E. Hsiao-Wecksler, E. Loth, G. Kogler, S. Manwaring, S. Tyson, K. Shorter, and J. Gilmer, "A pneumatic power harvesting ankle-foot orthosis

to prevent foot-drop," *Journal of neuroengineering and rehabilitation*, vol. 6, p. 19, 07 2009.

[11] M. N. A. Bin Ab. Patar, M. Mali, M. H. Mohd Ramli, A. K. Makhtar, and J. Mahmud, "Simulation and performance evaluation of a new type of powered dynamic ankle foot orthosis," in *2011 IEEE Colloquium on Humanities, Science and Engineering*, pp. 167–171, 2011.

[12] V. Bartenbach, M. Gort, and R. Riener, "Concept and design of a modular lower limb exoskeleton," in *2016 6th IEEE International Conference on Biomedical Robotics and Biomechatronics (BioRob)*, pp. 649–654, 2016.

[13] M. N. A. Ab Patar, A. F. Said, J. Mahmud, A. P. P. Abdul Majeed, and M. A. Razman, "System integration and control of dynamic ankle foot orthosis for lower limb rehabilitation," in *2014 International Symposium on Technology Management and Emerging Technologies*, pp. 82–85, 2014.

[14] "Military disability made easy.com: Ankle joint overview."

[15] "Exrx.net: Body segment data - kinesiology mean segment weights."

[16] "How do force sensitive resistor (fsr) sensor work?."

[17] "Fsr03ce product information page."

[18] "Adafruit: Force sensitive resistor - using an fsr."

[19] "Vytaflex 20 product info page."

[20] "Medicapteurs: Baropodometry - study of static or dynamic foot pressures."

[21] "Finding optimal rotation and translation between corresponding 3d points."

[22] "Github: Wpi-aim/aim-vicon python library."